UNIVERSIDAD DE CONCEPCIÓN
FACULTAD DE FARMACIA
PROGRAMA DE DOCTORADO EN CIENCIAS Y TECNOLOGÍA ANALITICA

DESARROLLO DE METODOLOGÍAS ELECTROANALÍTICAS BASADAS EN ELECTRODOS MODIFICADOS CON NANOMATERIALES DE C/Au PARA EL ANÁLISIS DE MATRICES AMBIENTALES COMPLEJAS

POR SAMUEL FELIPE PIÑA HODGES

Tesis presentada a la Facultad de Farmacia de la Universidad de Concepción para optar al grado académico de Doctor en Ciencias y Tecnología Analítica

Profesores guía: Dr. David Rodrigo Contreras Pérez
Dr. Ricardo Andrés Salazar González

Marzo, 2022

Santiago, Chile

TABLA DE CONTENIDOS

INDICE DE TABLAS

INDICE DE FIGURAS

RESUMEN

En la presente tesis se reporta el desarrollo de metodologías electroanalíticas basadas en electrodos confeccionados con una estructura hibrida de nanomateriales de carbono y oro para el análisis de contaminantes electroactivos con diferente naturaleza química: los isómeros orgánicos 1,4-dihidroxibenceno o hidroquinona y 1,2-dihroxibenceno o catecol en agua potable, agua de rio y en un RIL vitivinícola; y por otro lado se logró la determinación de arsenito en un efluente secundario de una planta de tratamiento, el cual fue tratado mediante electrocoagulación para la remoción de este contaminante y donde fue posible realizar el seguimiento del tratamiento utilizando la metodología desarrollada.

Experimentos realizados mediante espectroscopia UV-visible, dispersión dinámica de luz (DLS), microscopia electrónica de transmisión (TEM) confirmaron la síntesis de las nanopartículas utilizadas en la confección de los sensores utilizados. Posteriormente, análisis de voltametría cíclica (VC) y microscopia electrónica de barrido (SEM) permitieron confirmar el aumento del área electroactiva de los electrodos nanoestructurados.

Mediante VC se caracterizó la señal electroquímica de los analitos, obteniendo sus potenciales y corrientes de pico correspondientes a los procesos anódicos estudiados que sustentan la detección electroquímica de los analitos mediante voltametría de pulso diferencial (DPV), técnica electroanalítica en la cual se basaron ambas metodologías desarrolladas en esta tesis doctoral. También fue posible comprobar mediante estas técnicas la actividad electrocatalítica de las nanopartículas de oro sintetizadas. Se utilizaron como técnicas de referencia cromatografía liquida de alta eficiencia (HPLC) y espectrometría de absorción atómica con horno de grafito (GFAAS) para validar las metodologías electroanalíticas desarrolladas para hidroquinona-catecol y arsénico, respectivamente.

En ambas metodologías fue posible el análisis directo de los contaminantes en matrices medioambientales estudiadas, utilizando un electrodo heteroestructurado de nanopartículas de oro soportadas en nanotubos de carbono aminados de pared múltiple.

ABSTRACT

This thesis reports the development of electroanalytical methodologies based on electrodes modified with a hybrid structure of carbon and gold nanomaterials for the analysis of electroactive pollutants with different chemical nature: the organic isomers 1,4-dihydroxybenzene or hydroquinone and 1,2-dihroxybenzene or catechol in drinking water, river water and in a viticultural liquid industrial waste; on the other hand, the determination of arsenite was achieved in a secondary effluent of a wastewater treatment plant, which was treated by electrocoagulation for the removal of this contaminant and where it was possible to monitor the treatment using the developed methodology.

Experiments carried out using UV-visible spectroscopy, dynamic light scattering (DLS), and transmission electron microscopy (TEM) confirmed the synthesis of the nanoparticles used to make the sensors. Subsequently, cyclic voltammetry (CV) and scanning electron microscopy (SEM) analysis confirmed the increase in the electroactive area of the nanostructured electrodes.

Using CV the electrochemical signal of the analytes was characterized, obtaining their peak potentials and currents corresponding to the anodic processes studied that support the electrochemical detection of the analytes by differential pulse voltammetry (DPV), electroanalytical technique on which both methodologies developed in this doctoral thesis were based. It was also possible to check the electrocatalytic activity of the synthesized gold nanoparticles by means of these techniques. High performance liquid chromatography (HPLC) and graphite furnace atomic absorption spectrometry (GFAAS) are used as reference techniques to validate the electroanalytical methodologies developed for hydroquinone-catechol and arsenic, respectively.

In both methodologies it was possible to directly analyze the pollutants in the studied environmental matrices, using an heterostructured electrode of gold nanoparticles supported on multi-walled aminated carbon nanotubes.

1. INTRODUCCIÓN

En las últimas décadas ha sido posible la síntesis, análisis y manipulación de materiales a escala atómica, molecular o macromolecular para el estudio y desarrollo de nuevas aplicaciones, donde la síntesis de nuevos nanomateriales es de particular interés debido que estas nanoestructuras presentan propiedades que las diferencian de sus versiones macrométricas: i) poseen una gran relación área-volumen y ii) presentan mejoras en sus propiedades físicas y químicas debido a que sus efectos cuánticos son más relevantes a escala nanométrica (RSC Publishing, 2013), entre sus principales propiedades a destacar.

Los nanomateriales basados en carbono han sido de especial interés para estudios realizados en la última década debido a que se han desarrollado métodos de síntesis más eficientes como *chemical vapor deposition* (CVD), además de que estos materiales poseen variedad de estructuras micro y nanométricas como carbono vítreo, fibra de carbono, nanotubos, nanoesferas,

diamante y grafeno, por mencionar algunos, que han popularizado el uso de materiales de carbono (Alshahrani et al., 2018; Masoum et al., 2014; Nigović et al., 2018; Tashkhourian et al., 2016a; Wong et al., 2018). Las propiedades de los nanomateriales de carbono son conocidas hace años, donde el grafeno ha destacado por sus prometedoras aplicaciones en electrónica, ciencia de materiales y en biotecnología destacando su alta resistencia mecánica y su buena capacidad de conducir la electricidad (Anuar et al., 2018; Lawal, 2018; Lee et al., 2018; R. Li et al., 2018; Rao et al., 2018; M. Wang et al., 2018; Wong et al., 2018), o los nanotubos de carbono (CNT) que han sido utilizados en biomedicina, remediación ambiental y en electroanálisis por su buena capacidad como adsorbente debido a su gran relación área-volumen, presentan disminuciones en los sobrepotenciales obtenidos en los procesos redox mediados por este tipo de nanopartículas, presentan gran estabilidad física y química y pueden ser funcionalizados y enlazado covalentemente con otras moléculas y nanopartículas para modificar sus propiedades químicas (Gupta et al., 2018; Hou et al., 2016; M. Kooshki, Abdollahi, et al., 2011; L. M. Peng et al., 2014; Punetha et al., 2017; Thirumalraj et al., 2017; H. Yang et al., 2012; Q. Zhou et al., 2006).

Por otro lado, las nanopartículas metálicas son nanoestructuras que poseen diámetros menores a 100 nm, las cuales han sido sintetizadas en variedad de formas y morfologías, como en nano flores, nano anillos, nanobastones, nano hojas, nano cilindros o nanoesferas metálicas, entre otras formas logradas sintetizar con éxito, presentando mejoras en la relación área-volumen y en la conductividad eléctrica (Afrooz et al., 2016; Bansal et al., 2016; Feng et al., 2018; K. Liu et al., 2017; López-Lorente, 2014; Pu et al., 2014; Wu et al., 2017; Y. Xiao et al., 2017; Y. Zhou et al., 2018). Entre los primeros estudios realizados para la síntesis de coloides de oro puro vía reducción de cloruros de oro fueron realizados por Faraday. En los últimos 20 años se ha logrado el dominio de la forma de la nanoestructura sintetizada y el tamaño de la nanopartícula, con un bajo costo relativo de síntesis (Afrooz et al., 2016; Bansal et al., 2016; M. Kooshki, Abdollahi, et al., 2011; López-Lorente, 2014), presentando mejoras en las eficiencias catalíticas en procesos redox (Belghiti et al., 2016; Feng et al., 2018; Zhai et al., 2013), han sido utilizadas en el encapsulamiento y transporte selectivo de fármacos (RSC Publishing, 2013), produce aumentos en las corrientes obtenidas por procesos redox (M. Kooshki, Abdollahi, et al., 2011; Tashkhourian et al., 2016a; L. Xiao et al., 2008) y además son resistentes a la deformación mecánica y a la corrosión.

Históricamente, el desarrollo de metodologías analíticas para el control de especies peligrosas en el ambiente y el ser humano ha sido determinante tanto para comunidades, organizaciones ambientalistas y agencias gubernamentales que legislan y regulan la presencia de especies peligrosas en el ambiente y alimentos, además de organizaciones internacionales que vigilan el impacto de contaminantes en el medioambiente y también la sociedad se ha involucrado directamente en los últimos años, donde la problemática medioambiental ha tomado más importancia respecto a los problemas climáticos derivados de la contaminación y también por las especies peligrosas que se podrían consumir en alimentos y aguas de origen natural (Ávila & García, 2015; Jrög Feldmann et al., 2009; Hussain & Kharisov, 2017). Entre las familias de contaminantes a abordar en este trabajo y que más alerta han generado en los últimos años se encuentran:

Metales pesados y metaloides: En los últimos años se han reportado diversos casos de contaminación en suelos, aguas y alimentos con Cd, Cu, Cr, Zn, As, Pb, Ni, Cd, Co y Fe en niveles de traza y ultra trazas producidos principalmente por la actividad industrial, minera y agrícola (Beckers & Rinklebe, 2017; Kroukamp et al., 2016; Ma et al., 2014; Mestrot et al., 2013).

Estas especies pueden ser acumuladas en diversos organismos vivos como algas, peces, moluscos, plantas, insectos y en el ser humano, provocando problemas al sistema inmune, sistema nervioso central, sistema digestivo, además algunas especies como Cd, Pb, Cr o As presentan alta toxicidad a niveles de ultra trazas presentando actividad mutagénica, cancerígena y siendo letal en bajas dosis (Skaldina et al., 2018). Estas especies son usualmente determinadas usando métodos volumétricos, métodos analíticos basados en fotometría de absorción atómica con llama (FAAS), espectrometría de emisión atómica acoplado a ionización con plasma (ICP-OES) y espectrometría de masas acoplado a ionización con plasma (ICP-MS) en procesos productivos; y por difracción de rayos X (DRX) o fluorescencia total de rayos X (TXRF) en el análisis prospectivo en terreno de muestras minerales sólidas (Jrög Feldmann et al., 2009; Hussain & Kharisov, 2017; Suvarapu & Baek, 2016).

Contaminantes orgánicos emergentes (COE): Son contaminantes orgánicos no reconocidos como tales o especies que previamente eran desconocidas y que en los últimos años han sido detectadas en el medio ambiente gracias al desarrollo de técnicas analíticas más sensibles y

selectivas. Los principales vectores de contaminación de COEs son principalmente: el uso doméstico e industrial de drogas, fármacos, productos de cuidado e higiene personal. La contaminación por COEs genera diversos problemas en el medio ambiente, como la acumulación de estos contaminantes en diferentes sistemas ambientales, promoviendo interacciones de estas especies con los diferentes sistemas y seres vivos con los que interactúan, generando en algunas especies la prevalencia de enfermedades de tipo cáncer o problemas metabólicos debido al contacto de estas especies con disruptores del sistema nervioso y endocrino (Candia-Onfray et al., 2017; Cui et al., 1999; Donini et al., 2018; Hussain & Kharisov, 2017; Taheran et al., 2018). Los métodos clásicos para la determinación de especies orgánicas en matrices ambientales o en alimentos se basan en la extracción y preconcentración de los analitos desde la matriz y el posterior análisis mediante cromatografía gaseosa (GC) o cromatografía líquida de alta eficiencia (HPLC), utilizando una estrategia analítica adecuada según la naturaleza química del analito y de la matriz estudiada. (*Electrochemical Strategies in Detection Science*, 2015; Hussain & Kharisov, 2017).

Contaminantes orgánicos persistentes (COP): Son contaminantes orgánicos y productos de degradación obtenidos por la interacción de contaminantes con los diferentes componentes del medioambiente, estas especies son resistentes a la foto y biodegradación, debido a esto existen dificultades para el abatimiento de estas especies con los tratamientos aplicados convencionalmente (Alharbi et al., 2018; Ávila & García, 2015; Y. Jin et al., 2017). Cabe destacar que existen contaminantes emergentes que también presentan problemas de resistencia a la biodegradación, por lo que existen COEs y resistentes que presentan como vectores de contaminación el uso cotidiano e industrial de fármacos, productos higiénicos, domésticos y agrícolas, donde finalmente terminan con la descarga de estos contaminantes en el alcantarillado o a cuerpos de agua natural, similar a los COEs (Alharbi et al., 2018). En general presentan toxicidad a bajas concentraciones, acumulándose en tejidos de seres vivos provocando alteraciones al sistema endocrino, inmunológico, cáncer o problemas al sistema nervioso central. Usualmente la determinación de COPs es realizada por HPLC o GC según diversos métodos de referencia presentados en normas ambientales chilenas e internacionales (Ávila & García, 2015).

En la literatura se han publicado diversidad de métodos para la determinación de metales pesados, COE y COP, basados en ICP-OES o FAAS principalmente en el caso del análisis de HM (J Feldmann, 2002; Jrög Feldmann et al., 2009; Kamyabi & Aghaei, 2016; Kroukamp et al., 2016) y en HPLC en el caso del análisis de COE y COP (Alharbi et al., 2018; Cui et al., 1999; Patel et al., 2014; Toothaker et al., 1987). Si bien estas técnicas permiten una determinación analítica confiable en matrices ambientales complejas como aguas naturales y suelos, estas metodologías presentan algunos desafíos a superar para un monitoreo medioambiental agil: i) requieren un prolongado tratamiento previo de muestra, como digestiones o extracciones para separar el analito de la matriz, ii) en el caso de las metodologías basadas en HPLC, estas generan altos volúmenes de residuos contaminantes, iii) requieren operaciones preanalíticas para preconcentrar el analito de interés y tiempos de análisis de varios minutos para una única determinación, iv) son metodologías que requieren la alteración o destrucción de la muestra y v) requieren profesional técnico calificado para la aplicación de la metodología y materiales desechables de un solo uso para una única determinación.

El uso de nanomateriales en electroanalítica se ha enfocado principalmente en la construcción de electrodos nanoestructurados para construir sensores con características mejoradas respecto a electrodos macrométricos, donde se han reportado distintas propiedades, entre las que se encuentran: (i) una mayor área electroactiva, (ii) un mejor transporte de masa hacia el electrodo, (iii) actividad electrocatalítica (iv) mejor sensibilidad y selectividad en la determinación de compuestos electroactivos, al comparar con las metodologías de análisis clásicas para estos analitos (Gupta et al., 2018; López-Lorente, 2014; RSC Publishing, 2013). Específicamente, las nanopartículas de oro (AuNS) con diferentes morfologías han sido ampliamente utilizadas para aumentar la sensibilidad de la corriente de pico en determinaciones electroanalíticas y para mejorar la transferencia de carga, logrando mejorar la selectividad de determinaciones realizadas respecto al uso de electrodos tradicionales de oro, logrando sensibilidades comparables a las obtenidas por métodos basados en HPLC o ICP-OES (M. Kooshki, Abdollahi, et al., 2011; López-Lorente, 2014; RSC Publishing, 2013). Por otro lado, se han reportado trabajos donde el grafeno y los nanotubos de carbono de pared múltiple (MWCNT) han sido utilizados en la modificación de electrodos convencionales y también en compositos

con grafito, nanotubos de carbono y nanoesferas de oro destacando interesantes propiedades como: i) mejoras en la sensibilidad y robustez en las determinaciones realizadas sobre matrices complejas, ii) presentan bajas corrientes capacitivas en una amplia ventana de potenciales, permitiendo mejor relación señal-ruido, iii) mejoras en la selectividad y robustez en la detección electroquímica de especies electroactivas con naturaleza química similar o en presencia de interferentes propios de la matriz analizada, iv) poseen una buena capacidad de funcionalización, permitiendo usar nanomateriales de carbono como soporte de otras nanopartículas para la obtención de superficies nanométricas heteroestructuradas con propiedades nuevas y v)ha sido posible detectar múltiples analitos de forma rápida en una única determinación utilizando estos nanomateriales (Lawal, 2018; J. Li et al., 2018; L. M. Peng et al., 2014; RSC Publishing, 2013; Wong et al., 2018).

Los métodos de calibración clásicos como la adición estándar, curva de calibración o patrón interno poseen como principal ventaja la simplicidad del método de mínimos cuadrados para lograr evaluar la relación entre una señal instrumental y la concentración de analito, además entregan una gran cantidad de información analítica relevante y permite una fácil interpretación

de la información entregada por la regresión. Sin embargo, estos métodos requieren una alta calidad de los datos para entregar un resultado confiable, ya que son poco robustos al tener datos con señales interferidas o al realizar medidas en matrices reales complejas (N. Kumar et al., 2014; López et al., 2015; Pomerantsev & Rodionova, 2010). Los métodos multivariados de análisis de datos son utilizados hace décadas en disciplinas como la física, ingeniería o economía (N. Kumar et al., 2014), sin embargo, presentan como principal complejidad la necesidad de un sistema computacional con capacidad de procesar grandes volúmenes de información ya que trabajan en modelos de regresión multivariantes sobre toda la información instrumental obtenida en el análisis, permitiendo la determinación simultanea de diferentes analitos de interés, al realizar la calibración en presencia de interferentes conocidos en la matriz a analizar, como en el caso de los métodos de calibración de orden 1, donde se pueden mencionar como ejemplos modelos de regresión basados en mínimos cuadrados parciales (PLS), regresión lineal múltiple (MLR) o regresión por componentes principales (PCR) (Diez et al., 2015; Escandar et al., 2014; Escandar & Olivieri, 2017; Gholivand et al., 2014, 2015; López et al., 2015), por lo que la aplicación de estos métodos al análisis de matrices complejas medioambientales ha aumentado debido al

amplio acceso a computadores capaces de trabajar con una alta densidad de datos, lo que permitiría la reducción de tiempos de análisis y los costos asociados al tratamiento de la muestra para aislar o separar el analito de la matriz y al desarrollo de nuevos modelos de calibración cada vez más variados que podrían aplicarse a datos electroanalíticos (Cavanillas et al., 2012; Diez et al., 2015; Gholivand et al., 2014; M. Kooshki, Abdollahi, et al., 2011; M. Kooshki, Díaz-Cruz, et al., 2011; N. Kumar et al., 2014; Masoum et al., 2014; Mohammadi et al., 2018; Ni & Kokot, 2008; Pravdová et al., 2002).

Teniendo en cuenta la información presentada, el uso de electrodos modificados con materiales nanoestructurados de oro (Au) y carbono (C) sería adecuado para el desarrollo de metodologías electroanalíticas que permitan el análisis de especies contaminantes en matrices ambientales complejas como aguas naturales o de interés medioambiental, ya que en las metodologías electroanalíticas reportadas en los últimos años se han presentado avances en la aplicación de estas metodologías a matrices ambientales, donde destacan el aumento de sensibilidades y selectividades analíticas comparables con los métodos utilizados según la normativa

vigente, disminución de los tiempos de análisis y costos operacionales al comparar con las técnicas de referencia. También, se propone que la información analítica obtenida por técnicas electroquímicas acopladas a análisis factorial y calibración multivariante podrían resultar en una aplicación optimizada de la técnica en sistemas que presentan un alto grado de interferencia química o un alto grado de interferencia debido al efecto matriz, pudiendo determinar selectivamente un analito en matrices ambientales complejas con mínimo tratamiento de muestra.

2. HIPÓTESIS Y OBJETIVOS

Hipótesis

"La interacción entre nanotubos de carbono funcionalizados y AuNP permitirá obtener electrodos modificados con mayor área electroactiva y sensibilidad en la determinación de arsenito y dihidroxibencenos en matrices acuosas de interés ambiental"

Objetivo principal

Desarrollar metodologías analíticas confiables basadas en electrodos modificados con nanomateriales de carbono y oro, que permitan determinar arsenito y dihidroxibencenos en matrices acuosas de interés medioambiental.

Objetivos específicos

- Sintetizar y caracterizar de nanopartículas de oro (AuNP) mediante diferentes técnicas.

- Estudiar y caracterizar electrodos de carbono vitreo modificados con materiales nanoestructurados de C y Au.
- Desarrollar y optimizar una metodología electroanalítica para la determinación de arsenito y dihidroxibencenos en agua de grado analítico.
- Desarrollar una metodología electroanalítica confiable que permita la determinación de arsenito y dihidroxibencenos en matrices ambientales reales.

3. ESTRATEGIA ANALÍTICA

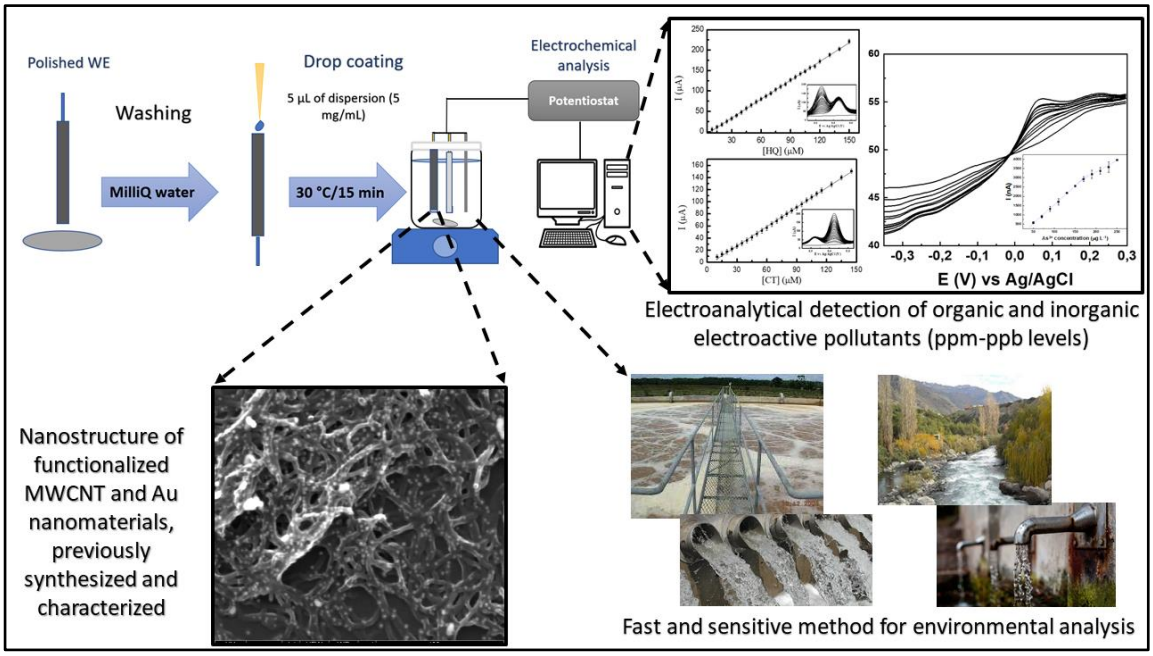

Figura 1: Resumen gráfico de la estrategia analítica utilizada en el desarrollo de esta investigación.

4. RESULTADOS

4.1. Glassy carbon electrode modified with C/Au nanostructured materials for simultaneous determination of hydroquinone and catechol in water matrices

En esta primera sección, se presentan los resultados publicados en la revista Chemosensors, en el trabajo titulado “Glassy Carbon Electrode Modified with C/Au Nanostructured Materials for Simultaneous Determination of Hydroquinone and Catechol in Water Matrices” (DOI: https://doi.org/10.3390/chemosensors9050088), publicado en mayo del 2021, donde se presentan resultados de esta tesis doctoral.

4.1.1. Introduction

In recent years, a large number of analytical methods have been developed based on the use of nanomaterials. These methods have a wide variety of applications in bioanalysis, clinical analysis, pharmaceutical analysis, food safety and environmental analysis (Gupta et al., 2018; H. Kooshki et al., 2018; Lawal, 2018; Qin et al., 2018). In particular, the use of nanomaterials for the modification of electrodes has generated great interest in environmental analytical chemistry. This is because, in general, these materials can significantly improve the conductivity and electrocatalytic activity of an electrical surface for a wide range of redox reactions, in addition to having broad potential window and low electrochemical reactivity (Govindasamy et al., 2018; Y. Li et al., 2019; C. Peng et al., 2018).

Carbon nanotubes (CNTs) are allotropes of carbon with a cylindrical nanostructure, in which a carbon-carbon link has a sp^2-sp^2 hybridization. Usually, CNTs have a nanometric-scale diameter and a micrometer-scale length, which gives them attractive chemical, mechanical and electronic

properties. In general, CTNs are divided into two groups: 1) Single-walled carbon nanotubes (SWCNT), and 2) multi-walled carbon nanotubes (MWCNT) (Odom et al., 1998; Wildgoose et al., 2006; Zakaria & Leszczynska, 2019). SWCNTs have a cylindrical nanostructure, formed by the winding of a graphite sheet in the form of a tube. In contrast, MWCNTs comprise several layers of concentrically ringed graphene, with a layer gap of 3.4 Å (Joseph Wang, 2005). CNTs have been widely used to modify electrode surfaces due to their unique properties, such as high electrical and thermal conductivity, high chemical and mechanic stability, high area-volume ratio and high adsorption capacity. In addition, their properties increase the sensibility of electrochemical sensors to detect organic and inorganic compounds (Nugent et al., 2001; Sedghi & Pezeshkian, 2015; Wong et al., 2015; Żelechowska et al., 2017). Moreover, the ease of immobilization and stability of proteins on CNTs have been widely used to manufacture electrochemical biosensors (Mendes et al., 2018).

Furthermore, the use of metallic nanospheres has also become widespread in electroanalysis (Campbell & Compton, 2010) due to their: i) high effective superficial area, ii) high mass transport, and iii) catalytic activity (Katz E &

Wang, 2004). Specifically, the study of gold nanospheres (AuNS) has been of interest because when they are deposited on the electrode surface, an increase in the charge transference and in the superficial area is observed, and high sensibility and selectivity is achieved when analyses are performed (Sebarchievici et al., 2016). One of the main ways of synthetizing AuNS is reducing a gold salt (generally $HAuCl_4$) in the presence of a stabilizing agent like citrate, through which the size and shape of AuNS can be controlled (Turkevich et al., 1951; Xia et al., 2010).

The determination of phenolic / polyphenolic compounds is a hot topic in the environmental, food and industrial fields (Ya Zhang & Zheng, 2007). Dihydroxybenzene compounds such as hydroquinone (HQ) and catechol (CT) are toxic (100 μM in lymphocyte/human) and persistent in the environment (W. Liu et al., 2012; Omar et al., 2016; Vilela et al., 2018). For this reason, it is important to develop simple and fast analytical methods that allow the determination of HQ and CT, which generally coexist in wastewater because they have a similar molecular structure and chemical properties. The determination of HQ and CT is carried out by spectrophotometric or chromatographic methods after separation

pretreatment processes, which requires long analysis times and large volumes of reagents. HQ and CT are electroactive compounds that can electrochemically oxidize on the surface of an electrode. The main difficulty in the simultaneous determination of both isomers lies mainly in the overlapping of the oxidation peaks, together with the loss of linearity in the voltametric response due to competition between the two compounds for the electrode surface. Both problems can be solved by modifying the working electrode. In the last years, many efforts have been devoted to develop modified electrodes able to increase the separation between both peaks together with the subsequent application of chemometric tools (Aragó et al., 2016).

The modification of electrodes using different nanomaterials has resulted in improved sensitivity for the determination of organic compounds in different matrices (Ghoreishi et al., 2012; Govindasamy et al., 2018) and has led to electroanalytical methodologies with detection limits at µM and even nM concentration levels (Bounegru & Apetrei, 2020; W. Jin & Maduraiveeran, 2017; Vytřas et al., 2018). Several methods have been reported for the quantitative determination of organics in water, such as gas and liquid

chromatography (Cui et al., 1999; Moldoveanu & Kiser, 2007), UV-Vis spectrophotometry (Elghobashy et al., 2016) and fluorescence (Patil et al., 2017). In these methods, detection limits between 0.1 and 1.0 µM have been achieved, but they exhibit some disadvantages such as complex pre-treatment of the sample and use of high volumes of organic solvents. In this sense, electrochemical methods have sensitivities comparable with those of spectrophotometric and chromatographic methods, can be miniaturized to perform on-site determinations of contaminants of interest, require inexpensive equipment for their implementation and enable the quantification of several analytes simultaneously in a short time (Ahammad et al., 2018; Karim-Nezhad et al., 2017; C. Peng et al., 2018).

In the present work, we studied the simultaneous determination of HQ and CT in real water using glassy carbon electrodes modified with three different multi-walled carbon nanotubes: i) non-modified carbon nanotubes (CNT), ii) carbon nanotubes modified with -COOH (CNT-COOH) and iii) carbon nanotubes modified with -NH_2 groups (CNT-NH_2), and decorated with gold nanospheres (AuNS). CNT-COOH and CNT-NH_2 produce better dispersion and increase the electrical conductivity of the modified electrode surface.

Amino group of CNT-NH_2 can interact with different materials and has an excessive reactivity. Among these nanomaterials AuNSs have been used as electrode materials due to their special properties in electrocatalysis of organic and inorganic compounds.

4.1.2. Materials and methods

Reagents and materials.

HQ and CT employed were of analytical grade, provided by Sigma Aldrich and used as received. Analytical grade water was used to prepare the solutions and dispersions. Boric acid EMPROVE®, glacial acetic acid EMSURE® and ortophosphoric acid EMSURE® were provided by Merck.

Glassy carbon electrodes (GCE, model CHI104) were modified using different multi-walled carbon nanotubes separately: carbon nanotubes without functionalization (CNT) and functionalized with -COOH and -NH_2 groups (CNT-COOH and CNT-NH_2, respectively), all of theme provided by Dropsens. CNT dispersions were prepared in an Elma S 10 Elmasonic ultra-sonic bath with a concentration of 1.0 g L^{-1} using water MilliQ as a dispersive agent. GCE were pre-cleaned by poolishing using alumina powder of 0.3 and 0.05 µm consecutively, and then washed with abundant Milli-Q water.

Gold nanospheres (AuNS) were synthesized using citrate as stabilizing agent following the Turkevich methodology using $HAuCl_4$ as precursor (Turkevich

et al., 1951). AuNS dispersions were prepared and then used to modify the GCE adding 10 µL on the electrode surface and then dried with nitrogen flux. AuNS were characterized by VIS-NIR spectroscopy using a Perkin Elmer Lambda 25 UV-VIS spectrometer, by Dynamic Light Scattering (DLS) using a NanoSizer-ZS Malvern Instruments, and by Transmission Electronic Microscopy (TEM) with a Philips Tecnai 12 Biotwin microscope. The mixture of the CNT and AuNS was characterized by SEM in a LEO 1420VP instrument with a coupled Oxford 7424 dispersive energy analysis instrument at an acceleration voltage of 25 kV.

For the simultaneous determination of HQ and CT, solutions at different concentrations of both compounds were prepared in a 0.1 M buffer Britton-Robinson solution at pH 2.0.

Electrochemical Measurements

Cyclic voltammetry (CV) and differential pulse voltammetry (DPV) experiments were performed on a CH Instrument potentiostat CHI1140C. For the qualitative and quantitative electrochemical analysis, 10 mL of the

solution were used in a traditional three-electrode electrochemical cell system. GCE with a geometric area of 0.126 cm^2 provided by CH Instruments were used as woeking electrode, $Ag/AgCl_{sat}$ as a reference electrode (CH Instruments) and platinum wire was used as counter electrode. In order to obtain the highest current response, different accumulation times were studied. Cyclic voltammograms were recorded between -1.0 and 1.0 V at a scan rate of 50 mV s^{-1}, under constant stirring at room temperature. The determination of HQ and CT performed based on their oxidation signal obtained by DPV with the following conditions: Step potential 4 mV, pulse amplitude 50 mV, pulse width 0.2 s, pulse period 0.5 s and deposition time of 30 s at 0.4 V as accumulation potential. The potential was scanned from 0.2 to 0.6 V. Electrodes do not need an activation and washing step previous to the DPV analysis.

Simultaneous determination of HQ and CT in different aqueous matrices by univariate and multivariate calibration

Four water samples of different types were obtained: i) MilliQ water, ii) drinking water, iii) industrial wastewater from a winery industry, and iv) river water. Subsequently, these samples were spiked with 50.0 µM of HQ and CT in the presence of 0.1 M Britton-Robinson buffer at pH 2. All the analyses were performed by DPV (10 mL of each solution) using standard addition method and a multivariate calibration by Partial Least Squares (PLS). PLS was developed by Hermans and Svante Wold applying pattern recognition methods to instrumental data obtained from chemical systems. The algorithm is based on a bilinear model that uses Single Value Decomposition (SVD) in matrix X that groups the voltamograms of each sample in relation to its concentration vector Y. Both matrices are decomposed into smaller matrices according to (Otto, 2017):

$$\boldsymbol{X = TP^T + E} \qquad \textbf{Eq. (1)}$$

$$\boldsymbol{Y = UQ^T + F} \qquad \textbf{Eq. (2)}$$

Where X and Y are the matrices of independent and dependent variables respectively, T and U are the matrices of scores containing orthogonal rows

to each other, P contains the loadings of matrix X and E is the matrix of (residual) errors of matrix X, Q corresponds to the loadings of matrix Y, and F is the error matrix of the vector Y. The B regression coefficients for the model are obtained according to:

$$\boldsymbol{B = W(P^T W)^{-1}} \qquad \textbf{Eq. (3)}$$

Where matrix W contains the weights obtained by PLS, and it is constructed by relating the values of each value of the vector Y (y_n=u) according to:

$$\boldsymbol{w^T = \frac{u^T X}{u^T u}} \qquad \textbf{Eq. (4)}$$

In PLS, the variables that show greater correlation with the response have an extra weight because they are more efficient in prediction. In this way, linear combinations of the predictor variables are chosen that are highly correlated with the response variables and that are able to explain the variation of the response as a function of the predictor variables. The decomposition of matrix X is independent from matrix Y, where the direction of each latent

variable of matrix X is modified until reaching the maximum covariance between this matrix and the concentration vector Y (N. Kumar et al., 2014).

Since the highest current response was obtained using the glassy carbon electrode modified with CNT-NH_2 and gold nanospheres (GCE/CNT-NH_2-AuNS), this electrode was used as working electrode for the DPV analyses.

4.1.3. Results and discussion

Determination of HQ using GCE modified with different CNTs

Cyclic voltammetry (CV) was used to characterize and studied towards HQ using the different CNTs in aqueous media. In order to obtain the highest current response, a previous pH study was performed in the range of 2.0 - 12.0 (data not shown), indicating that the highest current for both species is achieved at pH 2.0, so further analyses were carried out at this pH. **Fig. 2A** shows the voltammograms recorded using the different materials in absence of the HQ. An increase of the capacitive current was observed when a modified electrode was used. This increase was higher using the systems GCE/CNT-COOH and GCE/CNT-NH_2, followed by GCE/CNT. This change is related to the increase of the area of the modified electrodes and the better dispersion in water of the functionalized CNTs (Hu et al., 2019; Naqvi et al., 2020). Furthermore, in **Fig. 2A** several faradaic processes between -0.5 to 0.5 V can be observed in the CV profiles of electrodes modified with carboxylate CNTs. These signals have been reported in the literature and are due to the presence of electroactive functional groups, such as ketones or aldehydes, which are generated in the functionalization process of carbon nanotubes.

The intensity of these signals may interfere in the analyte detection process, generating the distortion of the peaks obtained by CV or DPV, especially in the reduction step. **Fig. 2B** shows the voltammograms recorded.

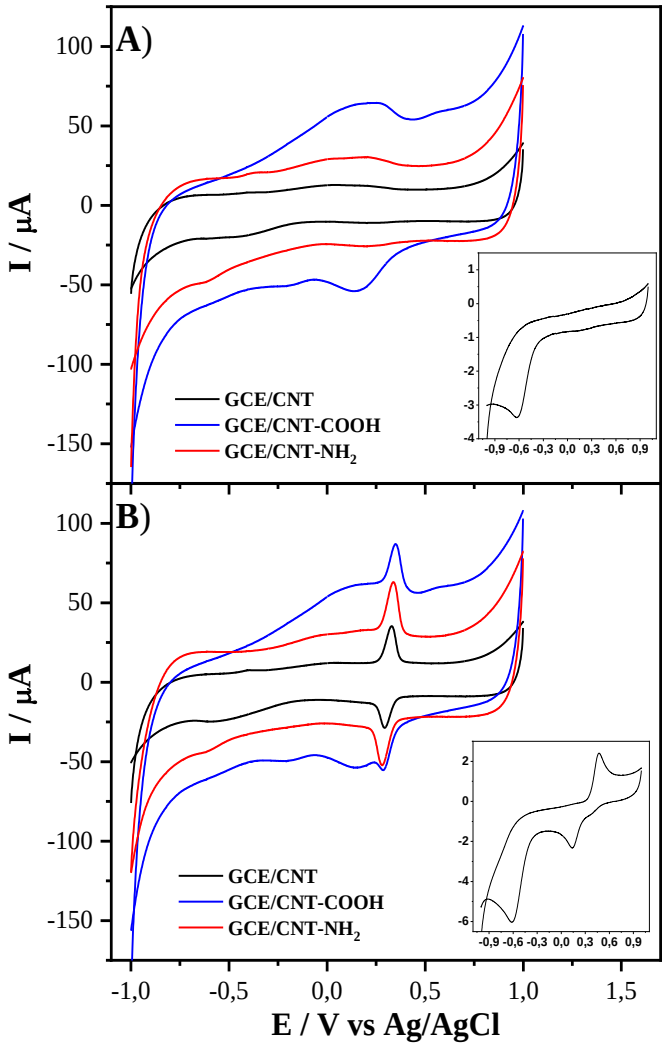

Figura 2. Cyclic voltammograms in the A) Absence, and B) in the presence of 0.1 mM of HQ using different electrodes (Inset: Cyclic Voltammogram of

bare GCE). Experimental conditions: electrolyte buffer Britton Robinson 0.1 M, pH 2.0, scan rate 50 mV s^{-1}, accumulation time 60 s.

In the presence of 0.1 mM HQ, an oxidation and reduction peaks corresponding to the formation of quinone (Q) and HQ can be seen (**Eq. 5)** using all the electrodes, however the intensity current for both oxidation and reduction peaks depends on the CNT used (Ganesh & Kumara Swamy, 2015) **(Fig. 2B)**.

$$HQ \rightleftarrows Quinone + 2H^{+} + 2e^{-} \qquad \textbf{Eq. (5)}$$

Additionally, the same figure shows a significant increase in the current peak for both oxidation and reduction peaks when CNTs are used; and this increase is higher when the CNTs are functionalized with -COOH and -NH_2 groups. An increase of 10.5 times and 13 times in the oxidation peak current compared to the GC electrode was observed using the GCE/CNT-COOH and GCE/CNT-NH_2 electrodes, respectively. However, there is a decrease in the resolution of the signals obtained with GCE/CNT-COOH, which may be attributed to the presence of sp^3 carbon that forms the bond between the functional group and the CNT wall, thereby affecting the electron transfer (Tserpes & Silvestre, 2014; Yang Zhang & Kang, 2018). The current and potential values for the redox process of HQ are summarized in **Table 1**.

System	Oxidation		Reduction		ΔE_p (V)
	Ep (V)	Ip (µA)	Ep (V)	Ip (µA)	
GCE	0.471	2.31 ± 0.04	0.139	-1.12 ± 0.03	0.332
GCE/CNT	0.328	23.26 ± 2.06	0.294	-19.99 ± 2.15	0.034
GCE/CNT-COOH	0.348	24.18 ± 2.36	0.286	-28.08 ± 2.41	0.062
GCE/CNT-NH_2	0.336	29.57 ± 2.44	0.281	-30.33 ± 2.35	0.055

Tabla 1. Current and potential values for the oxidation and reduction of HQ using the different systems of CNT. (Scan rate: 50 mV)

Table 1 also shows the ΔEp values. In the case of the electrode without modification, ΔEp is 0.332 V, which indicates that the process is irreversible. By modifying the electrodes with CNTs, the redox process becomes reversible, obtaining smaller ΔEp values close to the theoretical slope of Nernst (59.16 mV) (Compton, Richard G. Batchelor-McAuley & Dickinson, 2012). There are considerable differences in the ΔEp of the unmodified electrodes when compared to the electrodes modified with CNTs. First, a drastic decrease of the ΔEp can be observed when using electrodes modified with CNTs; therefore, the redox process becomes more reversible when using

nanotubes of carbon and shows an electrocatalytic effect on the reaction of HQ with the electrode surface. This could be attributed to the adsorption of HQ due to the functional groups present on the surface of CNTs (C. Yang et al., 2015).. Besides, the currents obtained by using electrodes modified with functionalized CNTs are higher than the currents obtained by using electrodes modified with CNTs.

Since the GCE/CNT-COOH and GCE/CNT-NH_2 systems present a higher current response, the following analyses were performed using only these systems.

Accumulation time effect on the oxidation of HQ

The effect of accumulation time on the current intensity was studied for the systems GCE/CNT-COOH and GCE/CNT-NH_2 (**Fig. 3**). For both systems, an increase of the current was achieved with the accumulation time, until reaching a maximum value and then, the current decays. The maximum current was achieved at 180 and 30 s for GCE/CNT-COOH, and GCE/CNT-NH_2 respectively. During the accumulation time, large amounts of HQ

molecules are rapidly adsorbed to the surface of the carbon nanotubes due to strong electrostatic forces at the start of the adsorption process. The decrease in current obtained after the optimal accumulation time can be explained due to the gradual occupation of the CNT surface by the HQ molecules, where a competitive adsorption is inevitable. The HQ molecules that are not absorbed diffuse from the outer Helmholz plane towards to the bulk of the solution, increasing the adsorption resistance and decreasing the adsorption rate of HQ. Furthermore, it can be seen that under the same conditions, CNT-NH_2 present a higher adsorption capacity, indicating that the conditions are favorable for HQ adsorption. This property would improve the migration of the analyte to the electrode surface, in addition to provide a larger surface for the accumulation and formation of double electrical layers, resulting in more sensitive electrochemical signals for the detection of these species in aqueous matrices. Accordingly, the following studies were performed using an accumulation time of 180 s and 30 s for the systems GCE/CNT-COOH and GCE/CNT-NH_2, respectively. Similar results were observed for the oxidation of CT under the same experimental conditions.

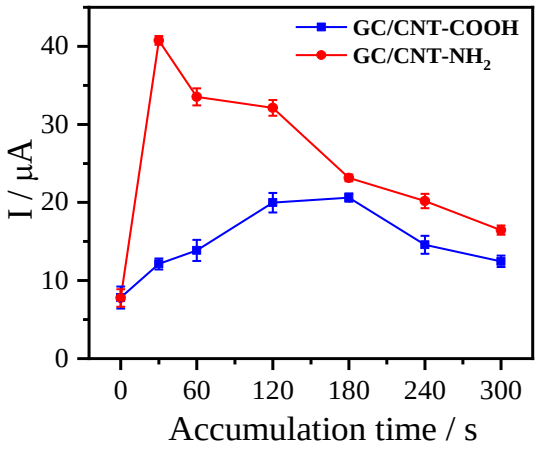

Figura 3. Effect of accumulation time on the oxidation current intensity of 0.1 mM HQ for the GCE/CNT-COOH and GCE/CNT-NH_2 systems. Working conditions: Scan speed 50 mV/s, Electrolyte: Buffer Britton-Robinson 0.1 M, pH 2.0.

Determination of HQ using GCE modified with different CNTs and AuNS

Before to use AuNPs in the electrochemical system, they were characterized by TEM, UV-Vis-NIR spectroscopy and Dynamic Light Scattering. TEM analyses (**Fig. 4A**) showed that AuNS present a homogeneous and quasi-

spherical shape, and their size is between 12-13 nm with an average size of 12.7± 2 nm. The size was confirmed by UV-VIS-NIR (inset Fig. 3A) analysis, which shown a maximum of the band at 518 nm. This value corresponds to a symmetric surface plasmon absorption and quasi-spherical particle of 12-18 nm (Alim et al., 2018a; Turkevich, John; Cooper, 1951). DLS analyses (**Fig. 5**) agrees the AuNS size with a 12.7 ± 2 nm value. The CNT-NH_2 and AuNS mixture was characterized using SEM (**Fig. 4B**), and images shown that AuNS are dispersed homogeneously on the CNT-NH_2 surface, which indicates a good interaction between the nanospheres and the amino groups present in the nanotubes, enabling the electrostatic deposition of the AuNS on the rough surface of the functionalized CNTs.

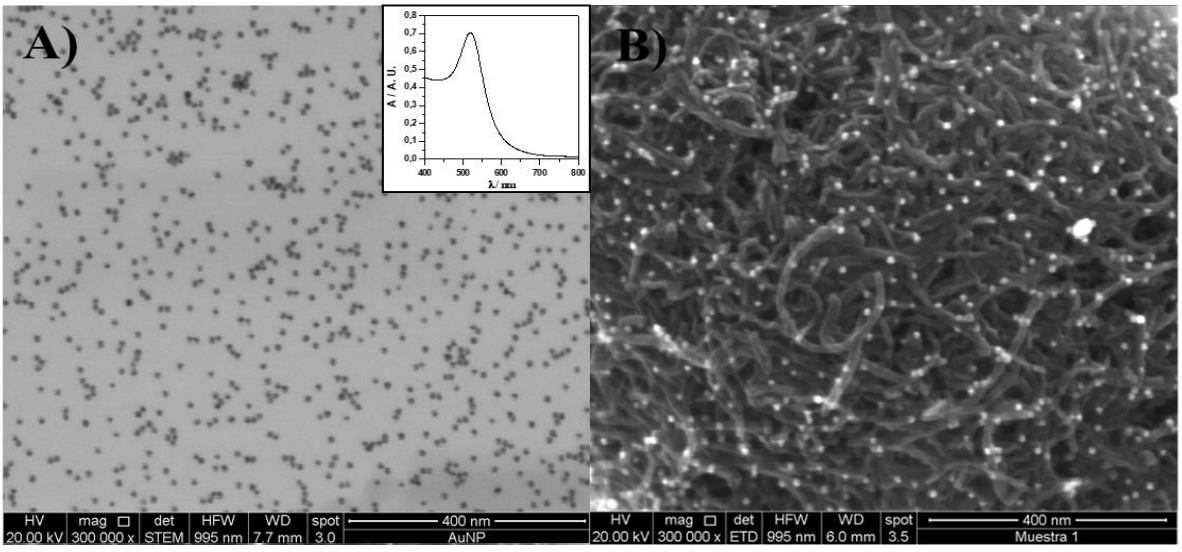

Figura 4. A) Transmission Electron Microscopy (TEM) and AuNS characterization, (Inset) VIS-NIR spectroscopy made for AuNS solution. Experimental conditions: Zeta potential: -20.3 mV. B) Scanning Electron Microscopy (SEM) made to GCE/CNT-NH_2-AuNS.

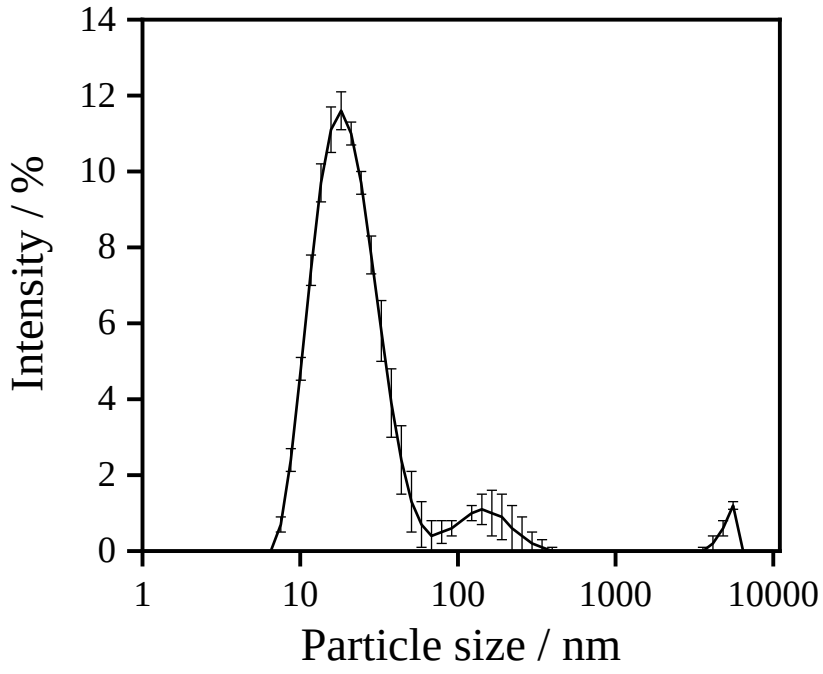

Figura 5. Size distribution of AuNS obtained using DLS.

The effect of the AuNS towards the HQ detection using CNT-COOH and CNT-NH_2 was studied using cyclic voltammetry (**Fig. 6A and Fig. 6B**

respectively). An increase of faradaic current was observed using AuNS and the different CNTs, however a more reversible and defined current peaks were obtained for the HQ/Q couple using GCE/CNT-NH_2-AuNS. As seen in **Fig. 6B**, a good interaction between AuNS and CNTs were assessed, which would create a synergistic effect on the HQ detection, thereby generating an increase in the current due to a better electronic transfer attributed to the contribution of both materials. The different peaks potentials and currents for the HQ oxidation using both systems are summarized in **Table 2**. A poor signal was observed using only GCE/AuNS (**Inset Fig. 6B**), which could be attributed to i) the incapacity of the surface of the GCE of adsorb AuNS due to the lack of functional groups that promote the electrostatic interaction between the nanoparticles and the surface of the electrode, and ii) AuNS present an smaller surface area compared to the electrodes modified with CNTs.

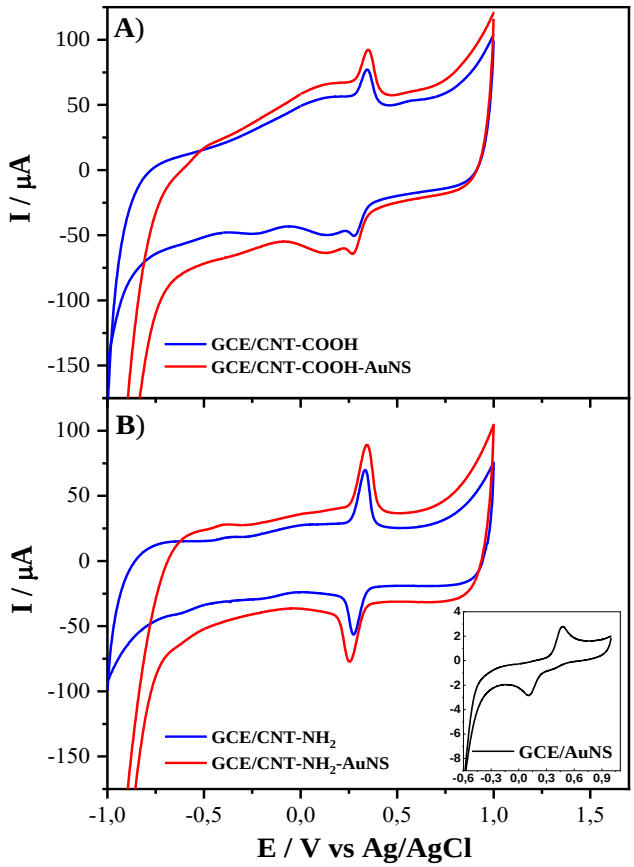

Figura 6. Cyclic voltammograms in the presence of 0.1 mM HQ using the different systems of CNT and AuNS. A) CNT-COOH (Inset: Cyclic Voltammogram of bare GCE modified with AuNS) with an accumulation time of 180 s, B) CNT-NH_2 with an accumulation time of 30 s. Experimental conditions: electrolyte buffer Britton Robinson 0.1 M, pH 2.0, scan rate 50 mV s^{-1}.

System	Ep (V)	Ip (μA)	System	Ep (V)	Ip (μA)
GCE/CNT-COOH	0.345	20.62 ± 2.41	**GCE/CNT-NH_2**	0.333	40.75 ± 2.47
GCE/AuNS	0.473	2.77 ± 0.03	**GCE/AuNS**	0.474	2.22 ± 0.04
GCE/CNT-COOH-AuNS	0.347	24.77 ± 4.11	**GCE/CNT-NH_2-AuNS**	0.343	45.47 ± 3.06

Tabla 2. HQ oxidation peak potentials and currents obtained using the different AuNS and CNT systems.

Since the highest current was obtained using GCE/CNT-NH_2-AuNS, the following experiments were performed using only this system

Simultaneous determination of HQ and CT using CNT/NH_2-AuNS

To assess the interference in the simultaneous determination of HQ and CT, we proceeded to study the oxidation of both analytes by DPV, considering that HQ and CT have an oxidation peak separated by 100 mV when analyzing each analyte alone using DPV. **Fig. 7A** shows the voltammograms of different HQ concentrations with a constant concentration of CT 50 μM. The peak current is increased linearly when increasing the concentration of HQ

in a range of 4.5 - 150.0 μM with R^2 = 0.996 and a F value = 0.0004 (F critical = 1.53, α = 0.05), with a linear equation of Ip (μA) = -0.278 + 0.154 [HQ] (μM). The same procedure was followed for the CT calibration curve, keeping a constant HQ concentration of 50.0 μM.

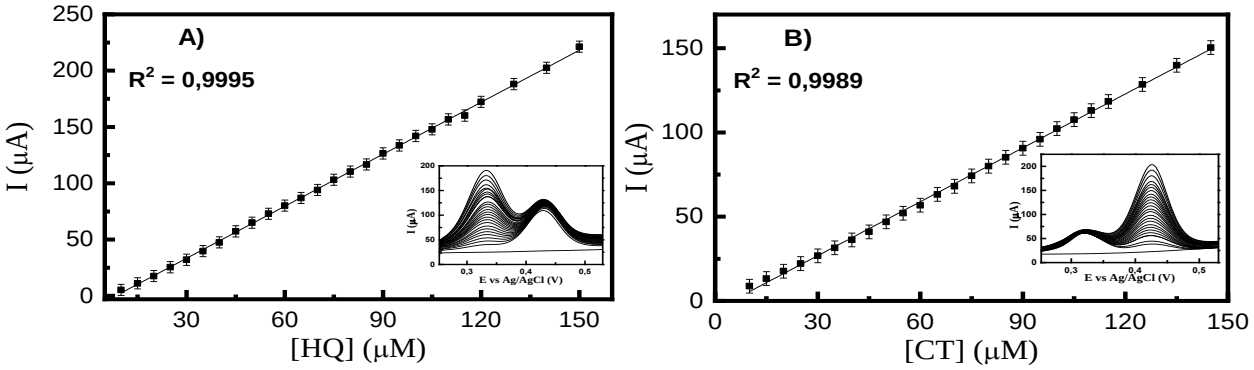

Figura 7. Oxidation voltammograms and calibration curve of A) HQ in the presence of 50.0 μM CT and B) CT in the presence of 50 μM of HQ Working conditions: Medium Britton-Robinson pH 2.0 Swept speed: 0.004 V s^{-1}, Accumulation time: 30 s.

In the differential pulse voltammograms in **Fig. 7B,** the peak current is observed to increase as the concentration of CT rises. In addition, the signal corresponding to HQ does not significantly affect the current intensity or the oxidation potential value in the measurements, having a separation peak of

>100 mV, approximately. The calibration curve for CT shows a good linear relationship in the presence of HQ, with a linear range between 4.0 - 150 μM and $R^2 = 0.998$ and a F value = 0.0026 (F critical = 1.53, α=0.05) according to equation Ip (μA) = - 0.514 + 0.107 [CT] (μM). In oxidation, the voltammograms of HQ and CT show a peak separation of 120 mV, which allows the differentiation of the compounds using the CNT-NH_2-AuNS electrode. A decrease in sensitivity during simultaneous determination can be observed when comparing the calibration curve of separated species. For HQ, the decrease in sensitivity is 0.531 μA μM^{-1}, and determination has an initial value (in the absence of CT) of 0.685 μA μM^{-1} (corresponding to a decrease of 77.5%). In the CT case, sensitivity decreases in the simultaneous determination of the analyte in the presence of HQ. Initially, without HQ, sensitivity was 0.677 μA μM^{-1}; however, when the solution contained 50 μM of HQ, a sensitivity of 0.107 μA μM^{-1} was achieved for CT, decreasing to 84.5%. Although peak potentials diverge above 100 mV, an overlap is seen between the signals when the HQ faradaic process ends and the CT oxidation process begins (between 0.400 and 0.420 V), which could decrease the sensitivity in the simultaneous determination of both isomers. The great decrease in CT sensitivity in the presence of HQ could be because HQ

oxidizes at lower potentials than CT. This redox process would interfere in the beginning of the oxidation of catechol. The experimental analytical parameters of the method were determined, and the results obtained from the validation are presented in the **Table 3.**

Material	Analyte	Sensitivity	Lineal range / µM	LD / µM	LQ / µM	Δ Ep (HQ-CC) / mV	Technique	pH	Ref
Graphene screen-printed electrodes	HQ	1.3221 µM	n.d.	2.7	9.1	105	DPV	7.0	(Aragó et al., 2016)
	CC	1.5825 µM	n.d.	1.7	5.6				
NDSBAC[1]	HQ	0.9997 µM	0.5 - 300	0.11	n.d.	112	DPV	6.5	(Zheng et al., 2020)
	CC	1.0662 µM	0.5 - 300	0.09	n.d.				
WBC/Au-850-15[22]	HQ	164.4 µA $\mu M^{-1} cm^{-2}$	0.008 - 1	0.002	n.d.	112.8	DPV	6.0	(Jinshou Wang et al., 2020)
	CC	132.0 µA $\mu M^{-1} cm^{-2}$	0.01 - 1.0	0.004	n.d.				
AuNPs-MPS[33]	HQ	n.d.	10.0 - 1000.0	1.2	n.d.	123	SWV	7.0	(Tashkhourian et al., 2016b)
	CC	n.d.	30.0 - 1000.0	1.1	n.d.				
GR-GO	HQ	n.d.	0.5 - 300	0.16	n.d.	102	DPV	7.0	(X. Zhou et al., 2014)
	CC	n.d.	0.5 - 300	0.2	n.d.				
NiO/CNT	HQ	n.d.	10 - 500	2.5	n.d.	~110	DPV	7.0	(Zhao et al., 2018)
	CC	n.d.	10 - 400	2.5	n.d.				
GO–TT–CNT	HQ	n.d.	0.01 - 200	0.035	n.d.	n.d.	DPV	7.4	(Han et al., 2014)
	CC	n.d.	0.5 - 200	0.049	n.d.				
CNT-NH_2-AuNS	HQ	0.154 µA μM^{-1}	4.5 - 150.0	1.3	4.3	100	DPV	2.0	This work
	CC	0.107 µA μM^{-1}	4.0 - 150.0	1.1	3.9				

Tabla 3. Comparison of different sensors reported for the simultaneous determination of HQ and CT.

[1] Nitrogen-doped activated carbon derived from sugarcane bagasse.

[2] Gold nanoparticles decorated the seedling of white myoga ginger-derived biochar.

The limit of detection (LD) and the limit of quantification (LQ) were calculated using the modern definition of IUPAC (Currie, 1995; Olivieri, 2015), which considers type α and β errors based on the residual error of the calibration curve and the instrumental error (pure error) with a LD ≈ 1.0 μM and LQ ≈ 4.0 μM. The linear range selected for the determination of analytes ranges between 4.00 - 150.00 μM. We studied accuracy of the CNT-NH_2-AuNS electrode in n = 15 determinations, obtaining a coefficient of variation of 2.2% for HQ and 2.1% for CT, which showed similar precision in a succession of repeated measurements for both analytes.

Comparing the results for the simultaneous determination of HQ and CT with electrodes modified with other materials reported in the literature (Table 3), the electrode modified with GCE/CNT-NH_2-AuNS achieves a higher sensitivity, good lineal range and a comparative △Ep in comparison with those obtained with electrodes modified with similar materials.

[3] Gold nanoparticles mesoporous silica modified carbon paste electrode

Considering the conducted studies and the electroanalytical response obtained with the GCE/CNT-NH_2-AuNS electrode, we worked on the simultaneous determination of these dihydroxybenzene isomers in a real matrix.

Determination of HQ and CT in different aqueous matrices

HQ and CT were determinate in different aqueous matrices which are from natural: drinking water, winery wastewater and river water. Standard addition analyses were performed since this type of calibration strategy is used for the analytical determination in matrices that have a considerable matrix effect and an external calibration is not allowed. A comparison of the standard addition results obtained in each matrix was conducted.

In this case, DPV was employed for the analysis of aggregated hydroquinone using the methodology developed in this work. The method developed was applied to the deter- mination of hydroquinone in different aqueous matrices, which are both of natural origin and water treated for consumption. The

determination of hydroquinone and catechol were performed by differential pulse voltammetry, obtaining the results shown in **Table 4**. The linear range of the analyte in the matrices studied was smaller than the working range obtained using standard MilliQ water. In addition, a reduced slope can be observed when determining the analyte in all the matrices. Recovery values under 88.4% were obtained in all the studied matrices, except for winey water, which has a very low recovery rate (less than 53.0%). The low recovery for fortified winery wastewater can be attributed to the effect of the matrix on determination, and there may be species that are consuming the hydroquinone added in the sample. In addition to this, all the matrices present a high amount of unidentified interferents, such as inorganic ions, chlorides, polyphenols and organic species that could interfere with the electrochemical oxidation of the dihydroxybenzenes studied in this work. In this way, analyzing hydroquinone and its isomers would be possible, as well as molecules that have dihydroxy-benzenes groups present in their structure, with low accuracy.

Matrix	Analyte	Concentration (µM)	Obtained concentration (µM)	Recovery (%)
Drinking water	HQ	55.0	48.6 ± 0.7	88.4
	CT		45.3 ± 0.5	82.4
Viticultural wastewater	HQ	145.0	75.8 ± 0.8	52.3
	CT		71.5 ± 0.4	49.3
River water	HQ	100.0	80.3 ± 0.5	80.3
	CT		84.2 ± 0.6	84.2

Tabla 4. Standard addition determination of hydroquinone (n = 10) in different aqueous matrices by differential pulse voltammetry, recovery coefficients and experimental t ($\alpha = 0.05$) for each determination made.

Considering the obtained results, it was proposed to use the wine wastewater for the application of a multivariate strategy for the quantification of hydroquinone and catechol since this matrix is the one that presents the lowest recovery levels, and the matrix has a greater quantity of interferents that hinder the determination of analytes.

Reproducibility study of the modified electrode area with nanostructured material

Reproducibility assays were performed for GCE/CNT-NH2 and GCE/CNT-NH2-AuNS In addition, the response of an unmodified GCE was studied as a control. For the study of reproducibility, ten electrodes (n = 10) were modified independently to analyze a concentration of 50.0 μM of HQ in the same day. Table 5 resumes the current values and the variation coefficients for the analyses. A variation coefficient of 3.12, 9.03 and 13.51% was obtained for GCE, GCE/CNT-NH2 and GCE/CNT-NH2-AuNS respectively. This variability in the current measured could be attributed to the differences in the electroactive areas of the electrodes modified with the nanomaterials. CNTs are hydrophobic and, therefore, present difficulties to be scattered in water, despite the dispersions were sonicated in an ultrasound bath during one hour to minimize the agglomeration of the material. These agglomerates generate two effects: i) different agglomerates sizes, which implies that not always will be the same amount of nanomaterial on the electrode surface, and ii) reduced efficiency in current, due to the loss of nanomaterial behavior and prevails of the macrometric properties of carbon materials.

Electrode	I (μA)	CV%
GCE	1.31 ± 0.04	3.12
GCE/CNT-NH_2	27.0 ± 2.43	9.03
GCE/CNT-NH_2-AuNS	22.6 ± 3.06	13.51

Tabla 5: Current values obtained for independently modified electrodes (n = 10) for the oxidation of 50.0 μM hydroquinone by differential pulse voltammetry.

Evaluation of multivariate calibration method for simultaneous determination of HQ and CT

A model based on PLS was built for the determination of HQ and CT in industrial residues of the wine industry. Best results were obtained by applying a baseline correction and log10 to compensate the dispersion of the baseline current between each measurement made due to the reproducibility of the electrodes. Voltammograms were preprocessed, and a mean center was applied to avoid variation of the oxidation potential of HQ and CT between

the measurements for the fortified samples. Two latent variables were selected for the HQ model and 3 latent variables for the CT model. This number of variables exhibits the lowest validation errors by cross validation allowing a more accurate determination because this number of components delivers a lower residual error. In addition, the analytical figures of merit were obtained for each model based on the PLS model obtained. These results are presented in **Table 6.** From the information obtained from the multivariate model, HQ and CT can be determined simultaneously in a range of 1.0 - 126.0 μM for HQ and from 7.0 – 177.0 μM for CT, with calibration and validation errors close to 20% obtained by cross validation. The PLS model was evaluated using an 8-sample validation set for wine industry wastewaters, fortified with known analyte concentrations.

Analyte modeled	HQ	CT
Data Transformation	Baseline correction + Log10	
Data Preprocessing	Mean Center	
Latent variables (k)	2	3
% Explained variance	87.4	93.9
$\mathbf{n_{calibration}}$	21	21
Range (µM)	1.2-125.9	6.7-176.9
SEC	19.7	21.6
SEV	21.74	23.51
$\mathbf{r_{val}}$	0.869	0.884
$\mathbf{r_{cal}}$	0.910	0.921
$\mathbf{n_{validation}}$	8	8
SEP	9.9	8.4
$\mathbf{r_{prediction}}$	0.758	0.950

Tabla 6. Analytical figures of merit of the PLS models constructed for the simultaneous determination of HQ and CT.

Standard prediction errors (SEP) of 9.9% were obtained for HQ quantification and 8.4% for CT in simultaneous quantification of both analytes in the wastewater. The charts with the values of SEP, and the HQ and CT real concentration versus predicted concentrations of both analytes are presented in **Fig. 8**. This figure shows graphically the correlation between the known analyte concentrations (Y observed) and the concentrations predicted by the model (Y predicted), where the line represents the predicted ideal values when evaluating the voltammogram obtained by DPV in the vector of regression B, where a greater proximity of the points to the line indicates a good accuracy in the prediction of the concentration. According to the results obtained, the values predicted by the PLS model are concordant with the concentrations added to the real sample having a low prediction error.

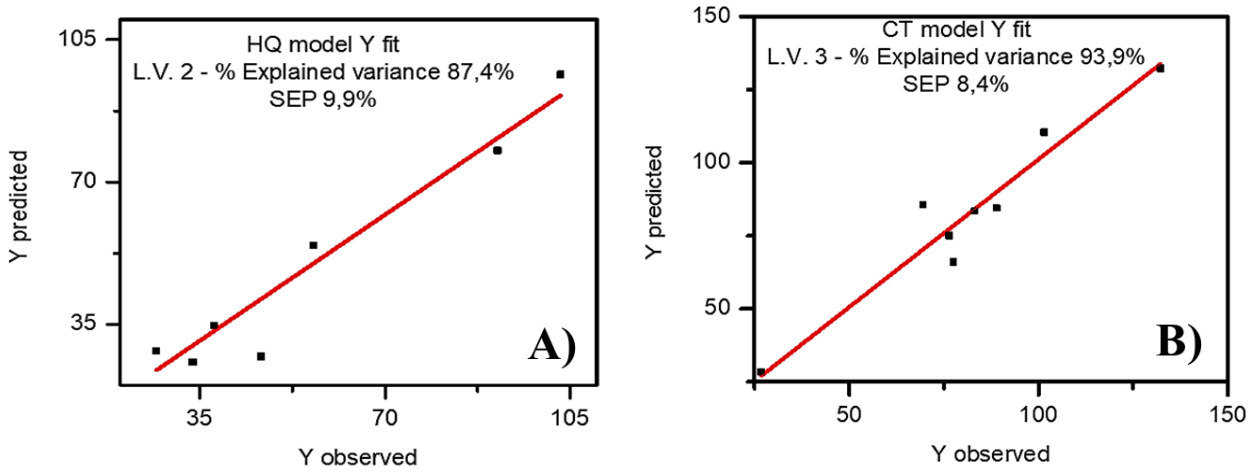

Figura 8. Plot of A) HQ and B) CT predicted concentrations as a function of the nominal values in validation samples for determination in wine industry wastewater by PLS calibration model.

Finally, the built model has high SEC and SEV values. This indicates, preliminary, that the model is not very robust for the simultaneous determination of HQ and CT. Nevertheless, a good correlation is observed between the values predicted by the models and concentrations used in sample fortifications when compared with standard addition in studies with real samples. To compare simultaneously the predictive capability of the studied methods, the predicted values obtained on this work are shown in **Fig. 9.** Elliptical Joint Confidence Region (EJCR) is employed to analyze the

performance of standard addition and PLS quantification in terms of normalized values of 1 for slope and 0 for intercept of each calibration methodology presented in this work and can include their confidence ranges around the means. The amplitude of the ellipse acts as a precision indicator, where a wide ellipse implies larger confidence intervals and a lower precision, and a small ellipse indicates a higher precision for that calibration method. Additionally, if the ellipse contains the normalized value (point located at {x,y}=1,0), it indicates graphically how accurate is the calibration method used.

Fig. 9 shows that the low accuracy and precision of standard addition makes it not suitable for the real samples. Instead, standard addition to analytical grade water combined with the PLS model yield more accurate predictions. The effect on bias is present in the ellipse obtained for the simultaneous quantification of HQ and CT in standard addition applied to real samples. Therefore, it can be inferred that there is an error produced by the matrix effect exerted by electroactive species that can interfere with the electrochemical determination, or by species present in the sample that can inactivate the electrode. This error would prevent the electronic transfer from

the analyte to the electrode and generate interference in the electrochemical signal from the redox process of HQ and CT. Regarding the precision of the methods, both the standard addition to MilliQ water and the determination via PLS are more accurate and precise than the simultaneous analysis of both dihydroxy-benzene isomers using standard addition in real samples. According to the results obtained, a multivariate methodology would be more suitable for the analysis of real samples, as they reduce the matrix effect on the determination of both analytes simultaneously and result in accurate and precise electrochemical determinations.

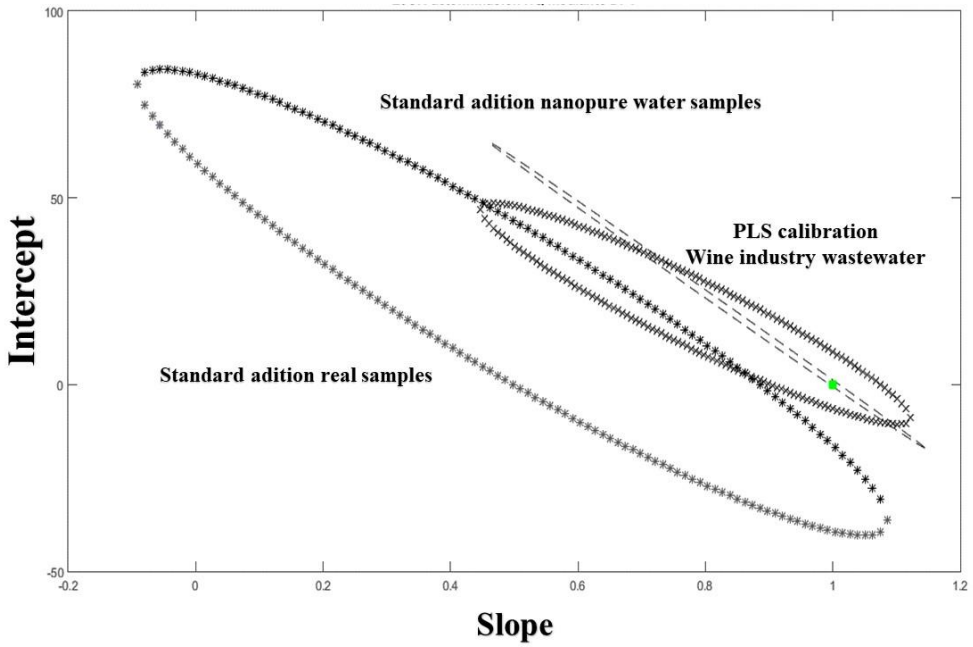

Figura 9. Elliptical joint region (at 95% confidence level) for the slope and intercept of predicted vs. nominal concentrations predicted by standard addition and PLS model developed in this work. The green cross marks the theoretical (intercept=0, slope=1) point.

The results obtained in this work indicate that chemometric multivariate calibration tools like PLS are adequate and better than classical calibration methods used in electrochemistry like standard addition for the direct and electrochemical simultaneous determination of HQ and CT in real samples, even in the absence of interference considered in the development of the methodology, which achieved errors lower than 10% in the quantification of the analytes.

4.1.4. Conclusions

The electrochemical oxidation of HQ in aqueous media showed a higher current response and lower ΔEp when using electrodes modified with multiple wall carbon nanotubes (CNT), oxidized multiple wall carbon nanotubes (CNT-COOH) and amino carbon nanotubes (CNT-NH_2), compared to the unmodified carbon electrode. The redox response of HQ presented a signal of higher current intensity when using electrodes modified with oxidized multiple-walled carbon nanotubes (CNT-COOH) and amine multiple-walled carbon nanotubes (CNT-NH_2), however the latter presented a more defined signal. The redox response of HQ increased by simultaneously modifying the electrodes with CNT-NH_2 and gold nanospheres (AuNS), further allowing separation with their structural isomers in the same solution.

An electroanalytical methodology was developed that allows the determination of HQ and CT in nanopure water, with a LOD of 1.0 μM in a working range of 4.0 to 150.0 μM, and an approximated error of 2.0%.

In real samples, the simultaneous determination of HQ and CT presented recoveries over 90% in drinking water and winery wastewater. A multivariate model was constructed by PLS, achieving prediction errors at 9.9% for HQ and 8.4% for CT with minimal sample treatment.

4.2. Electrochemical monitoring and removal of arsenic from secondary effluents through the electrocoagulation process

En esta segunda sección, se presentan los resultados de la investigación resultante como parte de esta tesis doctoral, trabajo enviado a la revista Chemosphere, el cual se titula “Electrochemical monitoring and removal of arsenic from secondary effluents through the electrocoagulation process”, sometido en marzo de 2022.

4.2.1. Introduction

Arsenic (As) is a toxic substance with a high environmental prevalence. It is estimated that more than one hundred million people around the world are exposed to unsafe levels of As or its compounds (Rodriǵuez-Lado et al., 2013). Arsenic can be found in the environment as: i) Organic As species, where arsenobetaine, monomethylarsonic acid (MMA), and dimethylarsinic acid (DMA) stand out. These species have low toxicity, but they tend to bioaccumulate in plants, cereals, algae, and animals (Jrög Feldmann et al., 2009; Promchan et al., 2016), and ii) Inorganic As species, predominantly pentavalent arsenic (arsenate, As^{5+}) and trivalent arsenic (arsenite, As^{3+}). Arsenite is one hundred times more toxic than arsenate in human beings (Jain & Ali, 2000) and it can also bioaccumulate as organic species (Abid et al., 2019; Antonova & Zakharova, 2016; Raab et al., 2016). Many international organisms, such as the World Health Organization (WHO), the United States Environmental Protection Agency (US-EPA), and the Directive of the European Environment Agency (EEA), have listed arsenic as a toxic substance of priority concern (EEA, 2013; Gorchev & Ozolins, 1984; US-

EPA, 2001). Therefore, a permissible limit of 10 μg L^{-1} of inorganic As in drinking water is highly recommended.

Anthropogenic contribution of arsenic in soil and underground water bodies is caused by mining, dye manufacturing, and agriculture (Garcia-Costa et al., 2021; Montefalcon et al., 2020),while naturally occurring arsenic contamination in water bodies derives from the dissolution of As-minerals like arsenopyrite, enargite, realgar, or tennantite (Guo et al., 2010; Xie et al., 2013). In this sense, the elimination of inorganic As species in water is mandatory. Different methodologies such as adsorption, membrane filtration, chemical coagulation, and electrocoagulation (EC) have been studied for this purpose (Asere et al., 2019; Sandoval et al., 2021; Syam Babu & Nidheesh, 2021).

In recent years, EC has proved to be an efficient process to treat groundwater and wastewater (Goren & Kobya, 2021; Nidheesh & Singh, 2017). Several advantages such as low sludge production, easy system set-up and operation, as well as inexpensive operating costs have increased the interest in it. In addition, EC can be applied directly in contaminated water if it has adequate

conductivity and pH values (Nidheesh & Singh, 2017; Sandoval et al., 2021). EC uses two metal electrodes immersed in the polluted water, which are connected to an external power source. An electric current is applied to the system which promotes the oxidation process at the anode generating metal cations (M^n). Simultaneously, H_2O molecules are reduced to hydroxide ions (OH^-) at the cathode. Pollutants are neutralized by coagulating agents [$M(OH)_n$ type], which collide promoting the formation and growth of flocs that induce the removal of pollutants such as arsenic species (Sandoval et al., 2021).

Several studies have dealt with the depletion of arsenic in groundwater/wastewater using aluminum or iron as sacrificial electrodes (Goren et al., 2020; Goren and Kobya, 2021; Sandoval et al., 2021).

In turn, a variety of analytical methods has been developed to detect and quantify organic and inorganic arsenic species at low concentrations (Petursdottir et al., 2015; Urgast et al., 2014). For instance, inductively coupled plasma (ICP) allows for performing multi-element analyses, achieving trace and ultra-trace detection limits (Jr & Township, 2016). ICP has been compared to flame atomic absorption spectrometry coupled with

hydride generation or graphite furnace as a standard technique for environmental As control (Hung et al., 2004; Jain & Ali, 2000), However, ICP-based methods have some disadvantages (Hung et al., 2004; Ma et al., 2014), which makes it difficult to study numerous samples and to perform real-time and on-site analyses. In recent years, the use of electrochemical sensors not only has allowed for conduct in-situ but also limit of detection (LD) analyses with an order of magnitude of as high as μg mL^{-1} and ng mL^{-1} (Buffa & Mandler, 2019; Bullen et al., 2020; Trachioti et al., 2019; L. Xiao et al., 2008).

In this study, an electrochemical sensor based on a heterostructure built with aminated multiwalled carbon nanotubes (MWCNT-NH_2) and decorated with gold nanospheres (AuNP) is developed to assess and validate a new electroanalytical methodology for determining arsenite concentration in real effluents. Moreover, the removal of arsenic from municipal wastewater was studied through an electrocoagulation process fitted with aluminum and iron as sacrificial electrodes.

4.2.2. Materials and methods

Reagents

All chemicals used in this study were of analytical reagent grade. Arsenite trioxide, potassium chloride, potassium ferrocyanide, potassium ferricyanide, tetrachloroauric acid solution, sodium citrate dihydrate, sodium hydroxide, and boric acid were purchased from Sigma-Aldrich® (Santiago de Chile, Chile). Glacial acetic acid and orthophosphoric acid of EMSURE® grade were provided by Merck® (Santiago de Chile, Chile). Pure and functionalized multiwalled carbon nanotubes (MWCNT) and alumina polishing dispersion were supplied by Dropsens® (Asturias, Spain). All solutions were made using ultrapure water obtained from a Millipore Milli-Q system.

Fabrication of MWCNT-NH_2/AuNP sensor

A glassy carbon electrode (GCE) provided by CH Instruments® (Austin, Texas) was modified with pure NH_2/COOH functionalized multi-walled carbon nanotubes. MWCNT dispersions were sonicated in an Elma S10 Elmasonic ultrasonic bath for 30 minutes at 25.0 ± 0.1 °C, with a 1.0 mg mL^{-1} MWCNT concentration. Subsequently, gold nanoparticles were synthesized in a reflux system; 100 mL of 1.0 mM $HAuCl_4$ at 190 °C were reduced with 5 mL of 77 mM sodium citrate under constant stirring during 30 min until obtaining a deep red AuNP solution due to the $Au^{3+} \rightarrow Au^0$ reduction. Finally, the AuNP solution was filtered through 0.45 µm PVDF filter. The pH solution was adjusted to 8.0 using sodium hydroxide 0.1 M.

The hybrid material dispersion was performed by the addition of 1.0 mg of MWCNT in 1.0 mL AuNS solution. Then, it was sonicated during 2 h at 25.0 °C. It is worth mentioning that, in this phase, the red color of the AuNP solution disappears, which indicates the formation of a nanometric MWCNT/AuNS heterostructure. Before the deposition of 10.0 µL MWCNT/AuNS dispersion drops on the GCE surface, the electrode was

polished using 0.3 and 0.05 µm of alumina suspension, and then washed with Milli-Q water. Finally, the GCE was dried at 30.0 °C.

AuNP analyses were performed by UV-Vis spectroscopy using a Perkin Elmer Lambda 25 UV-Vis spectrometer was used to evaluate the respective spectrum of the synthesized nanoparticle; dynamic light scattering (DLS) and zeta potential were determined using a NanoSizer-ZS Malvern Instrument and were used to determine the size distribution and surface charge of the gold nanoparticles; and transmission electronic microscopy (TEM) was performed in a Philips Tecnai 12 Biotwin microscope, and used to examine the morphology of nanoparticles. The surface modified with the MWCNT/AuNP mixture was analyzed by scanning electron microscopy (SEM) in a LEO 1420VP instrument coupled to an Oxford 7424 dispersive energy analysis instruments, the resolution was improved by increasing the acceleration voltage (25 kV), this technique was used to examine the hybrid surface of the electrochemical sensor.

Electroanalytical measurements

All electroanalytical experiments were carried out in a 15 mL non-divided amber glass cell with constant stirring at 25 ± 2 °C. A Britton-Robinson buffer solution was used as supporting electrolyte, the solution was prepared using, in a specific order, boric acid, glacial acetic acid, and orthophosphoric acid at 0.1 M. Cyclic and differential pulse voltammetry were performed using an Autolab (Metrohm, Herisau, Switzerland) Potentiostat/Galvanostat PGSTAT 204 system. A glassy carbon electrode acquired by CH Instruments® (Austin, Texas) was used as working electrode (0.19 cm^2 geometrical area); a saturated Ag/AgCl (1.0 M) acquired from CH Instruments® (Austin, Texas) was used as reference electrode, and a platinum wire was used as counter electrode. The cyclic voltammograms were recorded from -1.0 to 1.0 V at 10 mV s^{-1}. The As^{3+} electrochemical determination consisted in a preconcentration stage that was performed at a working potential of -600 mV during 200 s (optimized conditions); afterwards, a differential pulse voltammetry phase was performed from -600 to 300 mV at 0.005 V, 0.05 V, 0.05 s, 0.2 s of step

potential, pulse amplitude, pulse width, and pulse period, respectively. It is important to highlight that the MWCNT-NH_2/AuNP sensor does not need to be washed or activated before the determination stage.

Municipal wastewater treatment

The secondary effluent samples were collected from two wastewater treatment plants “Aguas Andinas, Mapocho Trebal” (33°32’82’’S, 70°50’08’’W) and “Aguas Andinas, La Farfana” (33°28'32.0"S, 70°47'30.6"W) located in Santiago de Chile (Chile). The sampling was performed in July 2021. Wastewater samples were characterized in a previous work (Calzadilla et al., 2021). Their physicochemical parameters, namely color, turbidity, conductivity, total organic carbon, sulfates and nitrates are showed in **Table 7**. The samples were fortified with a 1000 mg L^{-1} arsenic trioxide standard. As concentrations were measured using a Graphite Furnace Atomic Absorption Spectrometry (GFAAS) (Thermo Scientific, Model iCE3000) at λ = 193.6 nm of selective hollow-cathode arsenic lamp.

Parameters	Unit	Initial Value
Color		Light yellow
Odor		Strong
Turbidity	(NTU)	7.72
Total Dissolved Solid	mg L^{-1}	1202
Conductivity	(μS)	2402
Absorbance at 280 nm	(UA)	0.375
Chemical Oxygen Demand (mg L^{-1})	mg L^{-1}	35.5
Total Organic Carbon (mg L^{-1})	mg L^{-1}	22.68
Total Chlorine	mg L^{-1}	0.06
Nitrate	mg L^{-1}	7.7
Sulfate	mg L^{-1}	8.17
Ammonium	mg L^{-1}	42.5

Tabla 7: Characterization of seccondary effluent, values taken from previous work of Calzadilla et al., 2021.

The electrocoagulation tests were carried out in a 300 mL electrochemical cell with slow constant stirring at 25 ± 2 °C. Initial arsenite concentration was 250.0 µg L^{-1}. EC tests were performed using iron and aluminum as electrode materials. The bare geometrical area and electrode gap were 6.0 cm^2 and 1.0 cm, respectively. EC experiments were performed at current densities (*j*) of 5, 6, and 7 mA cm^{-2} for each electrode material during 60 min.

Flocs characterization

SEM analyses were carried out in a high-performance JEOL JSM-6010 PLUS/LA analytical scanning electron microscope. The energy dispersive analysis of X-rays (EDA-X) was conducted using a JEOL detector, which was integrated into the SEM microscope. A small portion of the samples was deposited on a graphite tape that was supported on an aluminum sample holder. The analysis of the samples was carried out in vacuum. The elemental concentrations were also determined using energy dispersive X-

ray fluorescence (EDXRF). All measurements were carried out under vacuum conditions using a Rigaku Nex CG X-ray fluorescence spectrometer, and an X-ray tube with Pd anode. The X-ray diffraction analyses (XRD) of aggregates formed during EC process were carried out using a Rigaku Ultima IV X-ray Diffractometer. XRD patterns were measured using Cu $K\alpha_1$ radiation, applied at 30 kV and 30 mA of voltage and current, respectively. Each pattern was collected for a diffraction angle range of $5° < 2\theta < 80°$ and scanned at 2.0° min^{-1}. The Fourier Transform Infrared Spectroscopy (FTIR) analysis of precipitates was carried out using a Thermo Scientific Nicolet iS10 FTIR Spectrometer with diamond Attenuate Total Reflectance (ATR) sampling accessory and OMNIC Software.

Statistical analysis

Statistical analyses were performed with Origin software (2015 version, OriginLab, Northampton, USA). Factorial optimization studies were

performed with Modde software (7 version, Sartorius, Göttingen, Germany). The points in figures represent the average of four replicates and error bars correspond to the sample standard deviation of the mean (n = 4) with a statistical significance of $p < 0.05$. All voltammograms were preprocessed in Autolab (Metrohm, Herisau, Switzerland) NOVA 1.1 Software, using a Savitzky-Golay smoothing algorithm. Subsequently, the voltammogram was derived to improve the signal-to-noise ratio and resolution of the oxidation peak obtained.

4.2.3. Results and discussion

Electrochemical studies of MWCNT/AuNP-modified electrodes

Cyclic voltammetry studies were carried out using MWCNT, MWCNT-COOH, and MWCNT-NH_2-modified glassy carbon electrodes to define the adequate electrochemical performance for the determination of arsenite. It is important to note that an electrochemical preconcentration stage was previously conducted by means of the application of a -500 mV potential during 100 s. A pH analysis was performed between 2.0 and 7.0 to find the highest current response. This study was performed using a 0.1 M Britton-Robinson buffer as a supporting electrolyte with an initial pH value of 2.0; then, the pH value was adjusted using 1.0 M NaOH. The observed current variation as a function of pH value is shown in **Fig. 10**. The greatest current response was reached at pH 2.0, which is consistent with values reported by other similar works in which carbon materials were used to study the electrooxidation of As^0 to As^{3+} in aqueous media (Lalmalsawmi et al., 2020; Pereira et al., 2016a). When the pH value was increased, a rapid decay in the

current peak was observed due to the oxidation from As^{3+} to the non-electroactive compound As^{5+}. According to this study, a pH 2.0 was selected to carry out the cyclic voltammetry studies of 1.0 mg L^{-1} As^{3+}.

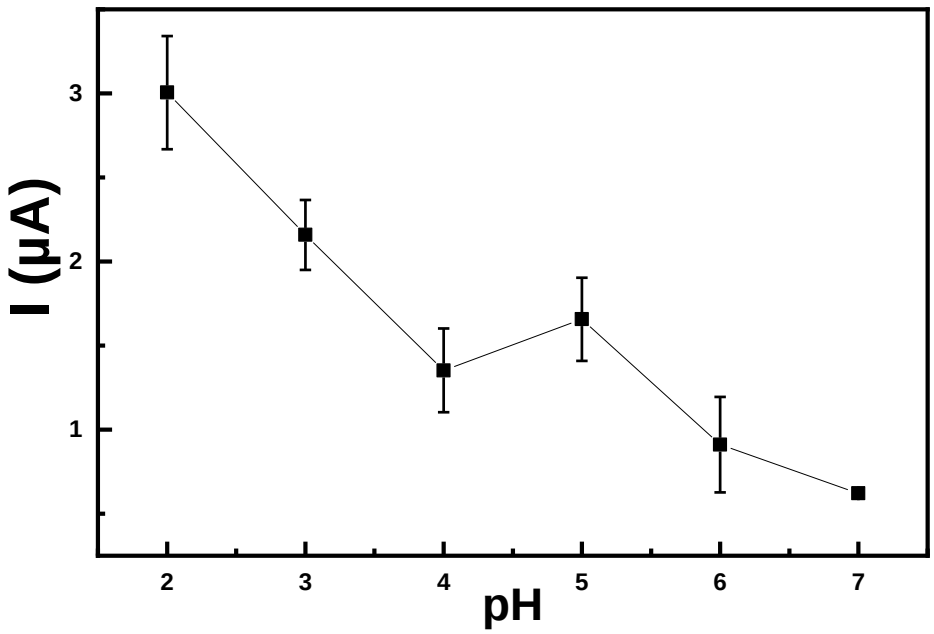

Figura 10: Observed arsenic cyclic voltammetry current variation as a function of pH value. As^{3+} 1.0 mg L^{-1} in Britton-Robinson buffer

Figure 11 shows the cyclic voltammogram of the blank. In this figure, an increased capacitive current is observed for all modified GCEs as a

consequence of their good electron transfer. MWCNT-COOH-modified GCE exhibited a wide anodic and cathodic faradaic signal between -500 and 300 mV, which is attributed to different functional groups present in nanotubes such as carboxyl groups, like non-selectively aldehyde and ketones groups produced during the functionalization of MWCNT.

The voltammograms performed with 1.0 M As^{3+} are displayed in **Figure 11B**. As it may be seen, they show a well-defined anodic signal when using GCE modified with MWCNT and MWCNT-NH_2, at 125 and 160 mV, respectively. The faradaic peak obtained with the MWCNT-NH_2-modified GCE was 1.88 times greater than MWCNT-modified GCE signal. The voltammogram of GCE modified with carboxylated MWCNTs presented anodic and cathodic faradaic peaks that correspond to the electroactivity of its oxidized groups. Therefore, the anodic signal obtained by arsenite oxidation was probably interfered by these electroactive carboxylated groups.

Finally, the electroactive area of all MWCNT-modified electrodes was studied using the Randles-Sevcik equation (Eq. 6):

$$I_p = 2.69x10^5\ n^{3/2}v^{1/2}D^{1/2}AC \qquad \text{Eq. (6)}$$

where I_p is the peak current (A), n is the number of exchanged electrons in $[Fe(CN)_6]^{3-/4-}$ redox pair (n = 1), v is the scan rate (5.0–500.0 mV s^{-1}), D is the diffusion coefficient of $[Fe(CN)_6]^{3-/4-}$ (D = 6.8x10^{-6} cm^2 s^{-1}), A is the electroactive area (cm^2), and C is the concentration of redox pair (mol cm^{-3}). The experimental A values obtained for unmodified GCE, MWCNT, MWCNT-NH_2, and MWCNT-COOH-modified GCEs were 0.08, 0.21, 0.35, and 0.39 cm^2, respectively. The augment of the electroactive area was between 4 and 5 times compared to the naked GCE.

Based on these results, aminated MWCNTs were selected to support the gold nanoparticles for the following studies, since they showed i) a better signal-to-noise ratio, ii) a better-defined faradaic peak during the oxidation of pre-concentrated As^0 to As^{3+}, and iii) a highlight increase in the electroactive area respect to naked GCE, unfunctionalized MWCNT, and MWCNT-COOH modified GCE.

Cyclic voltammograms of aminated MWCNT performed in As^{3+} 1.0 mg mL^{-1} showed a well-defined faradaic peak at 76 mV when the MWCNT-NH_2/AuNP electrode was used (**Fig. 11C**). An improvement in current intensity of 24.3 times compared to MWCNT-NH_2-modified was observed, which is attributed to the excellent electron transfer produced by the dislocation of surface electrons of AuNP. In addition, elemental arsenic forms stable amalgams with metallic gold and, therefore, the preconcentration stage should be more efficient when using the MWCNT electrode decorated with AuNP compared to one that has only a MWCNT nanostructure.

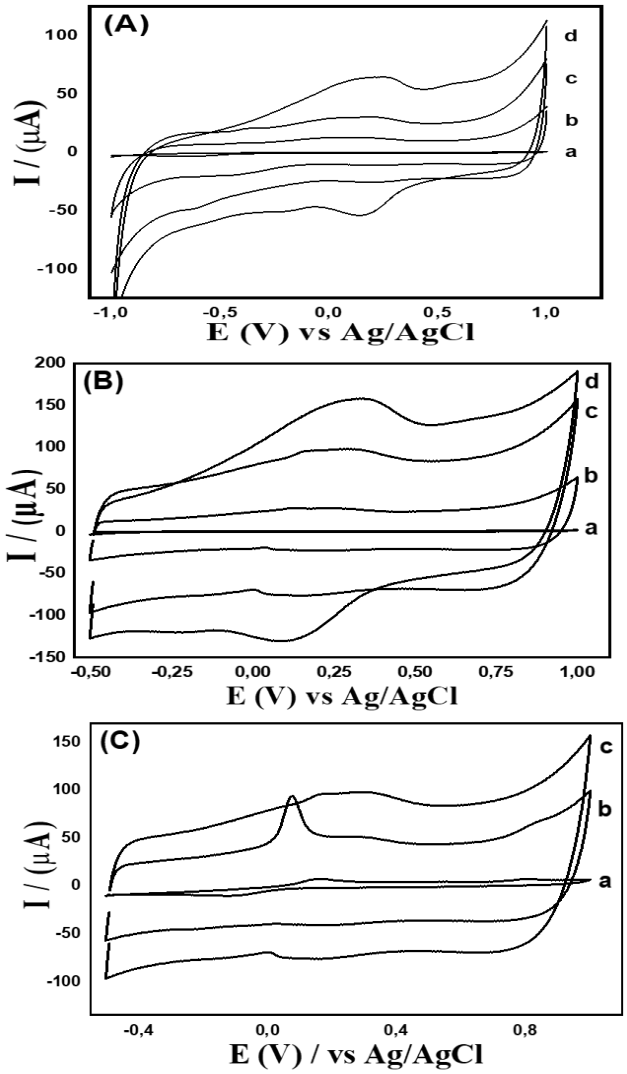

Figura 11: (A) Cyclic voltammograms of Britton-Robinson buffer pH 2.0 with a naked GCE (a) and modified GCE with MWCNT (b), MWCNT-NH_2 (c) and MWCNT-COOH (d); (B) cyclic voltammograms of As^{3+} 1.0 mg L^{-1} in pH 2.0 Britton-Robinson buffer with a naked GCE (a) and modified GCE with MWCNT (b), MWCNT-NH_2 (c) and MWCNT-COOH; (C) cyclic

voltammograms of As^{3+} 1.0 mg L^{-1} in pH 2.0 Britton-Robinson buffer with AuNP modified GCE (a) and MWCNT-NH_2/AuNP (b) and MWCNT-NH_2 (c) modified GCEs.

The morphology of the synthesized AuNPs was studied using TEM, DLS, and UV-VIS spectrophotometry. **Figure 12A** shows the TEM micrographs of synthesized AuNPs, which exhibited spherical morphology and homogeneous size with an average diameter of 12.6 ± 1.0 nm. The size of the nanoparticles was corroborated by a DLS analysis, obtaining a hydrodynamic diameter of 17.1 ± 1.8 nm. The difference in nanoparticle size is attributed to the fact that DLS allows for the measurement of the hydrodynamic diameter (Stokes diameter) of a hydrated and solvated nanoparticle. Therefore, the nanometric diameter size obtained by TEM corresponds to the net size of a gold nanoparticle, while that obtained by DLS corresponds to the size of a gold nanoparticle plus the solvation shell (citrate ion molecules) thickness of AuNP. Finally, UV-VIS spectrophotometry analysis showed a maximum absorption band at 518 nm which agrees with the surface plasmon of 12-18

nm quasi-spherical AuNPs (Alim et al., 2018b; Turkevich, John; Cooper, 1951).

SEM was used to examine the nanostructure obtained by modifying the GCE with aminated MWCNT (**Figure 12B**) and aminated MWCNT/AuNP (**Figure 12C**). The modified surface with aminated MWCNT exhibited a three-dimensional nanostructure of interconnected carbon nanotubes distributed on the modified surface in a random and homogeneous manner. This last confirms the increase of the electroactive area. A SEM micrograph of MWCNT/AuNP showed a distribution of carbon nanotubes like that obtained with aminated MWCNT. AuNPs were dispersed over the entire studied surface.

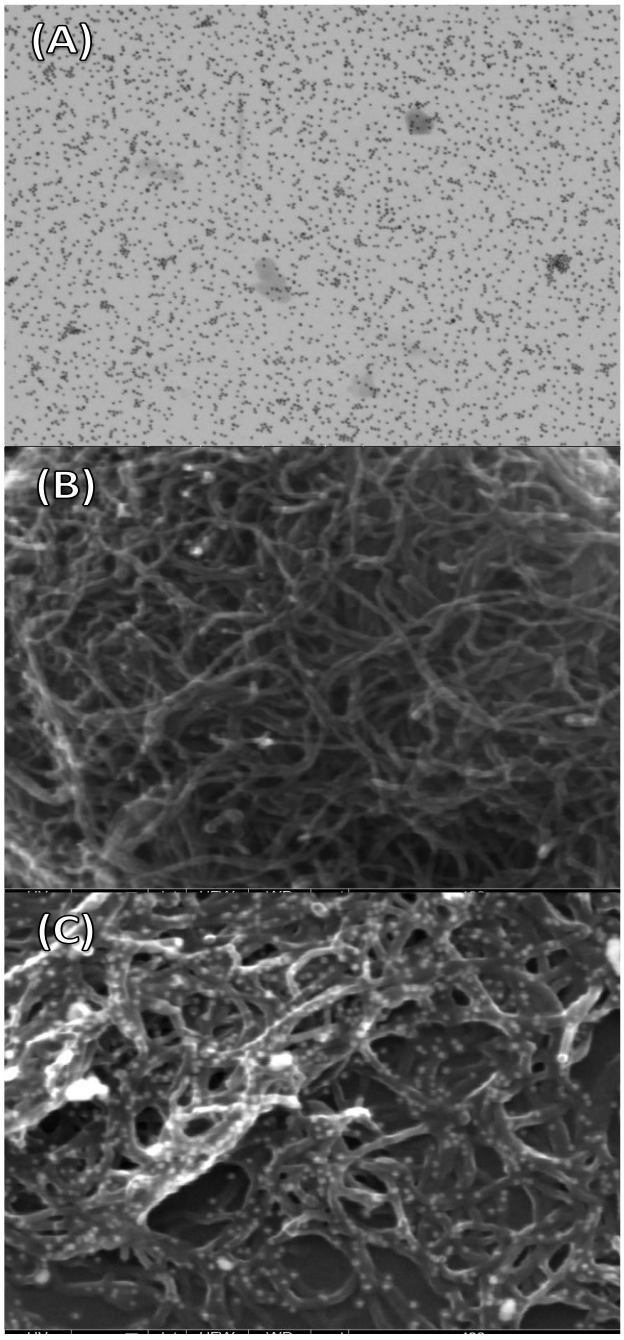

Figura 12: TEM micrography of AuNP (A); SEM micrographs of MWCNT-NH_2 (B) and MWCNT-NH_2/AuNP (C) modified GCEs.

Univariate and multivariate optimization studies of preconcentration stage

The electrochemical As detection is based on two steps: (1) a pre-concentration stage of inorganic As dissolved in a matrix that corresponds to the secondary effluent, which is carried out applying a fixed electric potential for a certain period of time, (2) a redissolution stage in which As is redissolved by monitoring the current obtained from the application of a potential sweep. The electrochemical reactions for both electroanalytical stages are presented in the following equations:

$$H_3AsO_{3\,(ac)} + 3H^+_{(ac)} + 3e^- \rightarrow As^0_{(ads)} + 3H_2O_{(l)} \qquad \text{Eq. (7)}$$

$$As^0_{(ads)} + 3H_2O_{(l)} \rightarrow H_3AsO_{3\,(ac)} + 3H^+_{(ac)} + 3e^- \qquad \text{Eq. (8)}$$

Figure 3 displays the univariate studies of two experimental factors at the optimization of preconcentration stage: accumulation time (t_{acc}) and accumulation potential (E_{acc}). These studies were carried out using an initial concentration of 300 µg L^{-1} As^{3+} in Britton-Robinson pH 2.0 media.

Differential pulse anodic stripping voltammetry (DPASV) was used to evaluate the effect of such studied parameters on the resulting anodic current from electrochemical oxidation of accumulated As^0 on a MWCNT-NH_2/AuNP surface. **Figure 13A** shows the influence of t_{acc} on the peak current of As^{3+} at -500 mV from 30 to 350 s. The anodic current increased rapidly during the first three minutes; then, the augment began to stabilize. This behavior was attributed to the As^{3+} present in solution which was electro-accumulated through two different mechanisms: i) the formation of Au-As nano-amalgams at the metallic nanoparticles surface and ii) the electroadsorption of As^0 in the aminated nanotubes network. The former mechanism is kinetically favored due to the electrocatalytic activity of the AuNPs (30-180 s), while the latter mechanism is slower, but possible, due to the large area-volume relationship, achieving the adsorption of analyte once the surface AuNPs are saturated and unable to amalgamate additional As^0. **Figure 13B** shows the effect of E_{acc} on the peak current in the interval between -700 and -400 mV using an accumulation time of 200 s. It was found that the optimal accumulation potential was -600 mV. However, by applying more negative potentials, the reduction of accumulated arsenic to arsenic

hydride, a non-electroactive compound, could be promoted, thus reducing the expected anodic signal of the oxidation from As^0 to As^{3+}.

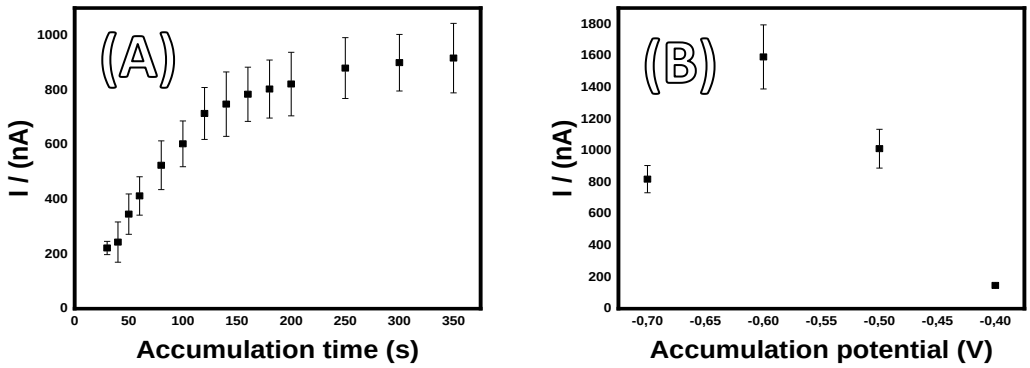

Figura 13: Monovariate studies of preconcentration factors t_{acc} (A) and E_{acc} (B) effect on arsenic peak current response obtained by DPASV in Britton-Robinson 0.1 M pH 2.0 media.

To determine the optimized conditions, a multivariate study was carried out using a Central Composite Face design (CCF), which allows for simultaneously analyzing both t_{acc} and E_{acc} variables with a low number of experiments. In addition, it is possible to detect interactions between the studied factors, which allows for optimizing the current response based on the applied quadratic model. **Table 8** shows the coded matrix of the CCF design used in this work. According to the experimental methodology of

multivariate analysis, multiple regression analyses were performed to calculate the polynomial equation that adjusts the studied variables with the current response.

Entry	X^*_1	X^*_2	X_1	X_2	Y
1	-1	-1	100	-0,7	0,356
2	1	-1	200	-0,7	0,627
3	-1	1	100	-0,5	0,303
4	1	1	200	-0,5	0,746
5	-1	0	100	-0,6	0,352
6	1	0	200	-0,6	1,325
7	0	-1	150	-0,7	0,649
8	0	1	150	-0,5	0,523
9	0	0	150	-0,6	1,164
10	0	0	150	-0,6	1,129
11	0	0	150	-0,6	0,816
12	-1	-1	100	-0,7	0,345
13	1	-1	200	-0,7	0,750
14	-1	1	100	-0,5	0,318
15	1	1	200	-0,5	0,841
16	-1	0	100	-0,6	0,416
17	1	0	200	-0,6	0,814
18	0	-1	150	-0,7	0,439
19	0	1	150	-0,5	0,450
20	0	0	150	-0,6	1,103
21	0	0	150	-0,6	0,978
22	0	0	150	-0,6	0,814

Tabla 8: Coded and operating variables for CCF model used for RSM optimization analysis of electrochemical preconcentration stage of As^{3+} on

MWCNT-NH_2/AuNP sensor. X_1 corresponds to t_{acc}, X_2 corresponds to E_{acc}, and Y corresponds to the peak current (*I*) in A. The response was obtained at DPASV stage (-600 to 300 mV range) corresponding to the peak current of electrochemical detection of arsenite (in µA)

The initial regression model was adjusted to include only significantly correlated coefficients, obtaining the following equation ($p < 0.05$):

$$Y\ (A) = 0.8911 + 0.2510X_1 + 0.0012X_2 - 0.3303X_2^2 \qquad \text{Eq. (9)}$$

where Y corresponds to the peak current (*I*) in A, and X_1 and X_2 are the coded variables related to t_{acc} and E_{acc}, respectively.

To corroborate the significance of the obtained model, regression coefficient (R^2) and Fisher's distribution (F-test) tests were performed. A R^2 value of 0.731 and an F value of 16.325 were obtained, which confirmed that the registered current responses were well fitted to the CCF model. The interaction X_1X_2 was not significant, P value = 0.555; therefore, the interaction was eliminated from the regression model. The weight of each parameter (**Figure 14**) studied in decreasing order as a function of the

regression coefficient values was t_{acc} >>>E_{acc}, which means that accumulation time is the principal factor in the electrochemical preconcentration stage.

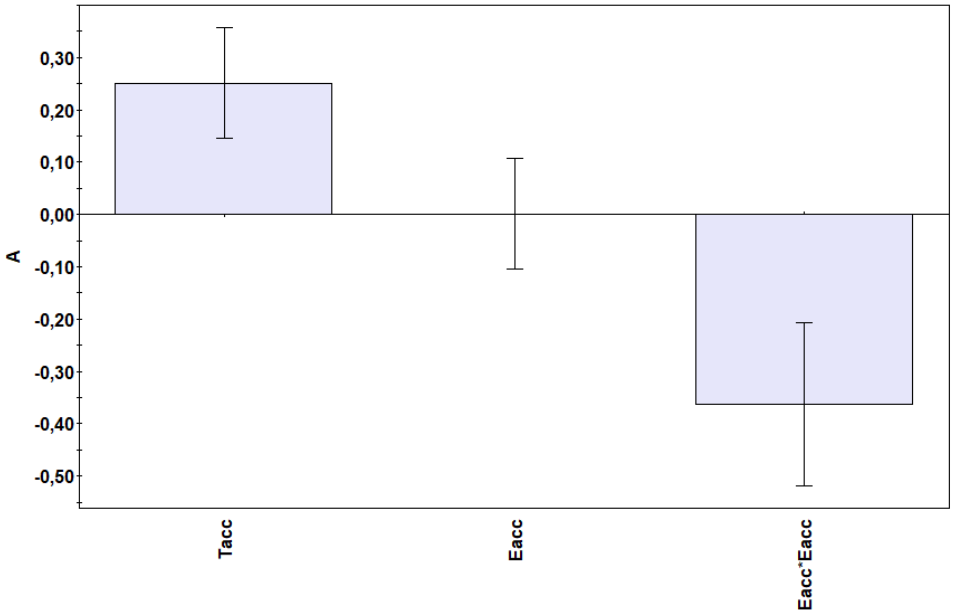

Figura 14: Coefficient plot of CCF model with confidence intervals in function of current response for 300 µg L^{-1} As^{3+} in Britton-Robinson pH 2.0. The data was centered and scaled to make the coefficients comparable.

Response surface methodology (RSM) has been used to determine the optimized experimental conditions. The contour plot and the obtained

response surface are exposed in **Figure 15**. In this case, the quadratic coefficient of E_{acc} becomes relevant at -600 mV from 30 to 300 s. The optimized parameters were 200 s and -600 mV for t_{acc} and E_{acc}, respectively. At these conditions a predicted peak current of 1.14 µA was observed using the MWCNT-NH_2/AuNP electrode for the analysis of As^{3+} 100 µg L^{-1} in Britton-Robinson 0.1 M at pH 2.0 media. This value was experimentally corroborated by DPASV obtaining 1.162 ± 0.028 µA (n = 5), and subjected to a t-test of statistical significance to evaluate if there is any statistical difference between the experimental and predicted response. A t value of -0.502 (t= 2.776, P = 0.05, 4 degrees of freedom). *t-value* is smaller than the critical value, then, there is no statistical difference between the value predicted by the RSM model and the experimental response obtained under optimized preconcentration conditions. Considering these results, t_{acc} = 200 s and E_{acc} = -600 mV were used in the validation of the analytical methodology for electrochemical arsenite quantification.

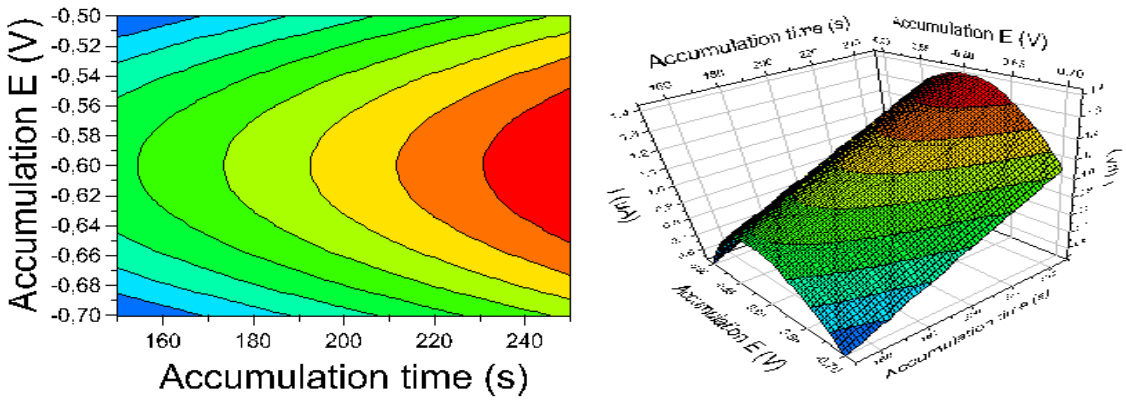

Figura 15: Contour plot (A) and response surface (B) generated from CCF design method using Eq. (9) for the peak current response optimization, obtained by DPASV after preconcentration stage.

External calibration studies for arsenite detection on real environmental matrix

Under optimized conditions, arsenite linear range studies were carried out using DPASV in fortified MilliQ water. As^{3+} concentration was studied from 50 to 1000 µg L^{-1} (**Figure 16**). A current response was obtained at -10 mV, being proportional to arsenite concentration between 50 and 300 µg L^{-1}.

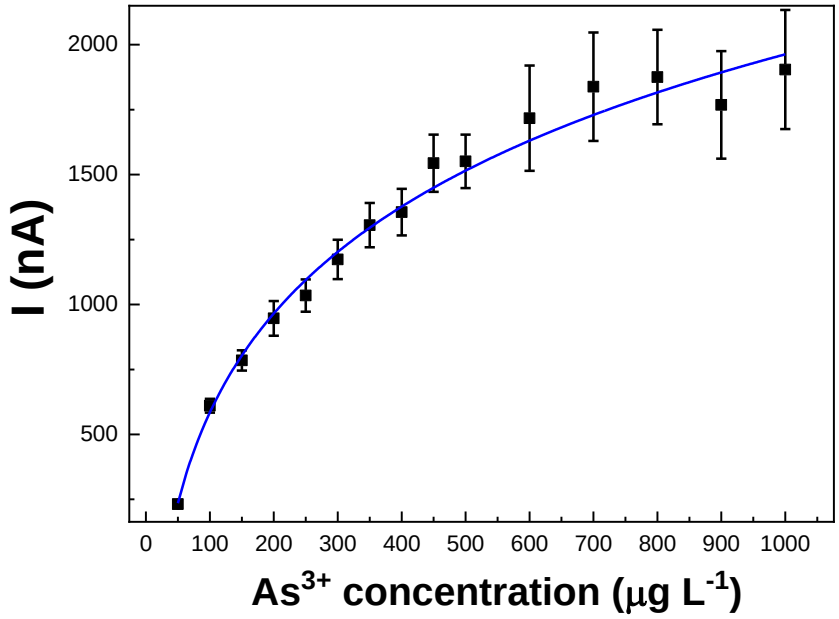

Figura 16: Arsenite linear range studies were carried out using DPASV in fortified MilliQ water. Working conditions: Britton-Robinson pH 2.0 media, tacc: 200 s, Eacc: -600 mV, DPV step potential: 0.005 V, DPV pulse amplitude: 0.05 V, DPV pulse width: 0.05 s and DPV pulse period: 0.2 s.

Figure 17A shows the DPAS voltammograms and the standard addition curves of arsenite in synthetic and real WWTP effluents located in Santiago de Chile, Chile. The following linear equation and coefficient of determination were obtained: $Y= 207.47 + 7.07X$, $R^2= 0.998$. Moreover, a

detection limit (DL) of 0.98 µg L^{-1} and a quantitation limit (QL) of 13.4 µg L^{-1} were found. DL and QL values were calculated with the Residual Sum of Squares (RSS, 0.61 nA), according to the currently accepted definition by IUPAC.

Using a real effluent, 8.0 mL were mixed with 2.0 mL of Britton-Robinson 0.5 buffer at pH 2.0 in an amber electrochemical cell of 15 mL volume. **Figure 17B** shows two different areas that present a directly proportional relationship between the anodic peak response obtained at 60 mV and As^{3+} concentration in the sample: i) from 50 to 170 µg L^{-1} ($Y = -417.73+ 19.58X$, $R^2 = 0.997$) and from 170 to 250 µg L^{-1} ($Y = 667.61 + 13.17X$, $R^2 = 0.997$). In addition, it was found that the determination of As^{3+} by DPASV in the effluent had a higher sensitivity than the same methodology studied by external calibration in MilliQ water, being 2.77 times more sensitive in the range between 50 and 170 µg L^{-1} and 1.86 times more sensitive in the range between 170 and 250 µg L^{-1}. The increase in sensitivity is attributed to the physicochemical characteristics of the real effluent, for example, higher electrical conductivity results in higher detected currents. DL and QL were calculated using RSS for the curve obtained from 50 to 170 µg L^{-1}, obtaining

values of 0.39 and 42.89 µg L^{-1} for DL and QL, respectively. Predicted QL value was verified by analyzing a fortified effluent sample with 43.0 µg L^{-1} of arsenite which produced a concentration of 43.13 ± 0.47 µg L^{-1} (n = 4), obtaining a *t-value* of 1.02 (t = 3.18, P = 0.05, three degrees of freedom), experimentally demonstrating the predicted QL.

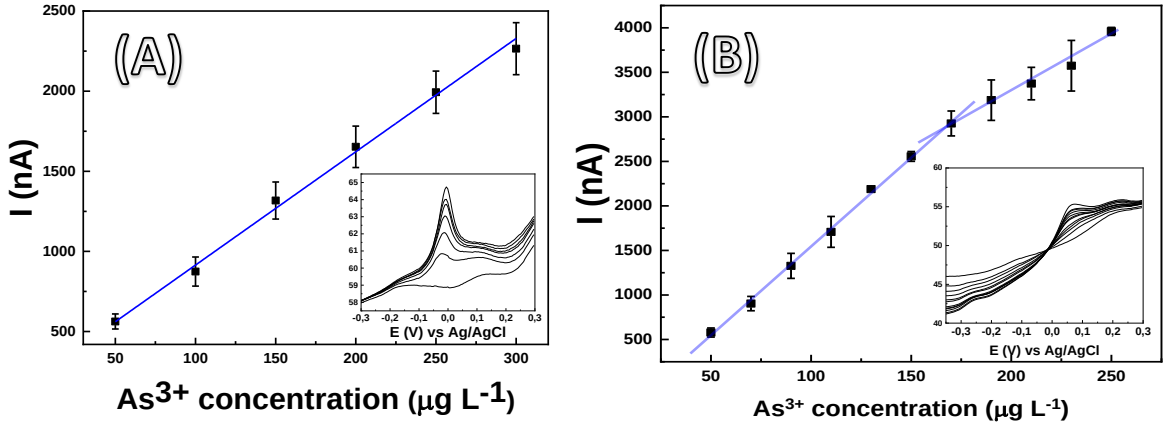

Figura 17: DPAS voltammograms (inset) and standard addition curves of As^{3+} in MilliQ water (A) and As^{3+} in real effluent water (B). Working conditions: Britton-Robinson pH 2.0 media, t_{acc}: 200 s, E_{acc}: -600 mV, DPV step potential: 0.005 V, DPV pulse amplitude: 0.05 V, DPV pulse width: 0.05 s and DPV pulse period: 0.2 s.

To assess the stability of the MWCNT-NH_2/AuNP sensor, 20 measurements were performed by standard addition to an effluent sample fortified with 100 µg L^{-1} of As^{3+}, obtaining a relative standard deviation of 3.76%. Recovery studies were carried out with 50.0 and 100.0 µg L^{-1} of As^{3+} and then assessed by GFAAS. Results are showed in **Table 9**. In all cases, recoveries between 99.1 – 102.6 % were achieved with the MWCNT-NH_2-AuNP sensor by DPASV analysis.

Matrix	**Added concentration (µg L^{-1})**	**DPASV**		**GFAAS**	
		Analyzed concentration (µg L^{-1})	Recovery (%)	Analyzed concentration (µg L^{-1})	Recovery (%)
Nanopure water	50.0	51.30 ± 0.51	102.6	48.15 ± 0.06	96.3
	100.0	100.24 ± 0.36	100.2	100,14 ± 0.02	100.1
Effluent water	50.0	49.55 ± 1.31	99.1	49.38 ± 0.08	98.8
	100.0	101.32 ± 0.72	101.3	100.71 ± 0.04	100.7

Tabla 9: Recovery assays of arsenite in water samples with MWCNT-NH_2/AuNP sensor by differential pulse anodic stripping voltammetry (DPASV) and reference technique (GFAAS).

Table 10 shows a comparison between the results of this study and results reported with other nanostructured sensors. MWCNT-NH_2/AuNP electrode used in this work achieved a wide linear range and low DL, showing good analytical performance for arsenite quantification in a complex real matrix. Considering the results obtained in the validation of the analytical method, it is possible to apply the MWCNT-NH_2/AuNP sensor to the EC treatment monitorization in a real contaminated effluent.

Electroanalytical technique	Sensor composition	Linear range	DL	Matrix	Referencia
LSASV	Au/SPCE	1 - 100 µg L^{-1}	0.03 µg L^{-1}	River and agricultural waters	(Punrat et al., 2013)
LSASV	Zn organometallic complex immobilized on polymeric beads	1 - 4 µg L^{-1}	0.3 µg L^{-1}	Groundwater	(Bullen et al., 2020)
LSASV	AuNPS functionalized polypyrrole nanowires	0.75 - 7.50 µg L^{-1}	0.37 µg L^{-1}	Tap water	(Salunke et al., 2021)

SWASV	AuNP in SPCE	20.0 – 150.0 µg L^{-1}	16.73 µg L^{-1}	Commercial apple juice	(Sullivan et al., 2021)
LSASV	Carbon paste and ThNP	3 – 180 µg L^{-1}	0.1 µg L^{-1}	Natural and drinking waters	(Pereira et al., 2016b)
DPAdSV	Carbon paste with carrageenan gel	0.50 – 6.70 µg L^{-1}	0.22 µg L^{-1}	River water	(Núñez et al., 2018)
DPASV	AuSiNP	0.5 – 12.0 µg L^{-1}	0.22 µg L^{-1}	Tap water	(Trachioti et al., 2019)
SWASV	AuCuNP	10.0 – 90.0 µg L^{-1}	2.09 µg L^{-1}	MilliQ water	(M. Yang et al., 2016)
CV	GO/Nafion/leucine	1000 – 5000 µg L^{-1}	500 µg L^{-1}	Tap wáter	(S. Kumar et al., 2016)
LSASV	Membrane CNT/AuNP	0.75 – 750.00 µg L^{-1}	0.75 µg L^{-1}	Tap water	(Buffa & Mandler, 2019)
DPASV	MWCNT-NH_2/AuNP	42.89 – 170.00 µg L^{-1}	0.39 µg L^{-1}	Water effluent	This work

Tabla 10: Comparison of different electrochemical sensors reported for arsenite determination

Application of MWCNT-NH_2 sensor for tracking arsenite during electrocoagulation treatment in real water effluents

Two electrocoagulation systems, based on aluminum and iron electrodes, were used to evaluate arsenite removal from polluted effluents.

A sample of 0.25 L of effluent (pH 7.8) contaminated with 250 µg L^{-1} As^{3+} was treated using two aluminum electrodes (6 cm^{-2} geometric area). Arsenite removal was monitored by DPASV during 1 h of treatment; standard addition was conducted every 20 minutes. **Figure 18A** shows the decay of As^{3+} concentration during the EC process at 15.0, 12.5 and 10.0 mA cm^{-2}. In this case, arsenite removal was not complete regardless of the current density applied in the aluminum EC treatment. As shown in **Figure 18A**, after one hour of treatment, a removal of 57.84 % of the arsenic present in the effluent was achieved at 10.0 mA cm^2, a 66.88 % removal with 12.5 mA cm^2 and the best performance was obtained using a j of 15.0 mA cm^2, removing 71.86 % of the pollutant present in the effluent.

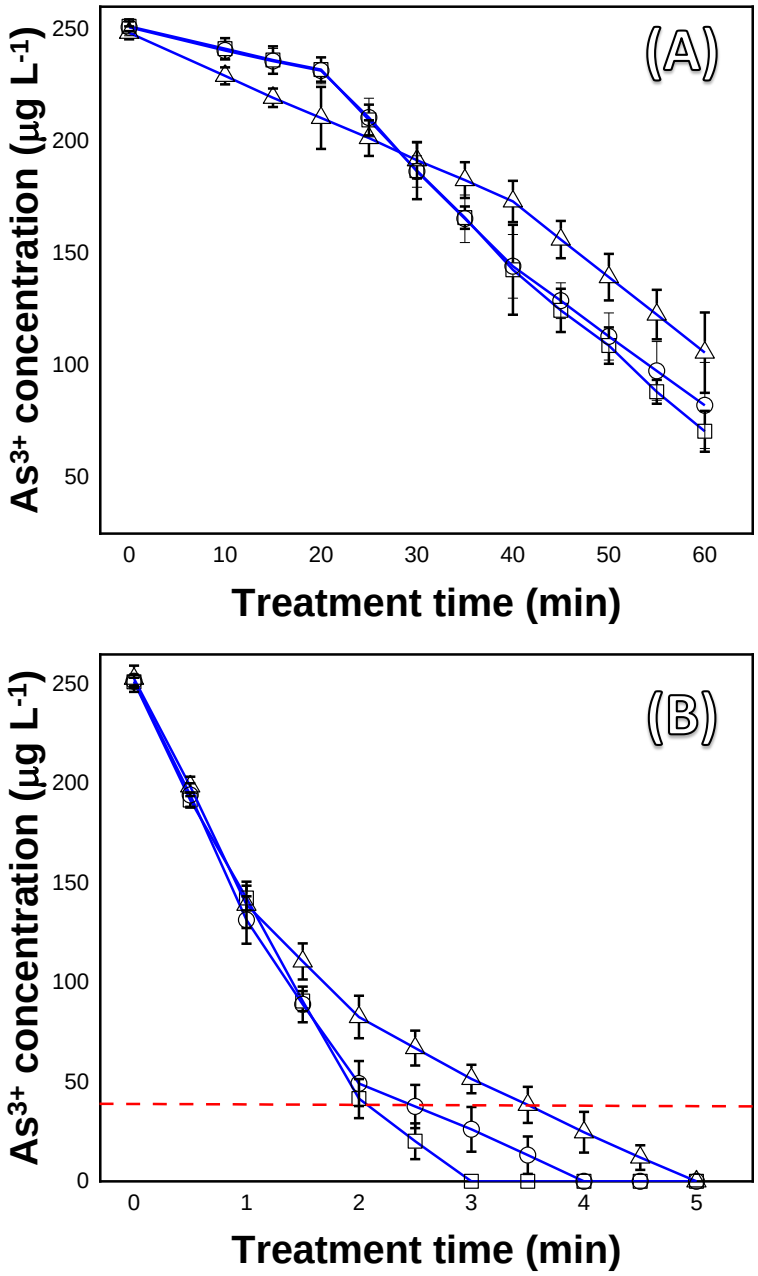

Figura 18: Arsenite abatement by EC of 0.25 L effluent sample contaminated with As^{3+} 250 µg L^{-1} at 25.0 °C and initial pH 7.80 using a pair of aluminum electrodes applying j of □ 15.0 mA cm^2, ○ 12.5 mA cm^2 y Δ 10.0 mA cm^2

(A) and a pair of steel electrodes applying j of □ 6.0 mA cm^2, ○ 5.0 mA cm^2 y Δ 4.0 mA cm^2 (B).

The main electrochemical reactions involved when employing aluminum electrodes are the following:

At the anode: $Al_{(s)} \rightarrow Al^{3+}_{(aq)} + 3e^-$ Eq. (10)

At the cathode: $3H_2O_{(l)} + 3e^- \rightarrow 1.5H_{2\,(g)} + 3OH^-_{(aq)}$ Eq. (11)

This kind of wastewater would promote the oxidation of arsenite to arsenate, through the combined oxidation of hypochlorite, added in the effluent treatment process, and by the applied current intensity during the EC process (Goren et al., 2020). After various intermediate reactions, insoluble aluminum oxyhydroxides species are formed. Then, the removal of arsenate is mediated by coprecipitation and adsorption processes according to:

$Al(OH)_{3\,(s)} + HAsO^{2-}_{4\,(aq)} \rightarrow [Al(OH)_3 * HAsO^{2-}_4]_{(s)}$ Eq. (12)

$$Al_2O_{3\,(s)} + HAsO_{4\,(aq)}^{2-} \rightarrow [Al_2O_3 * HAsO_4^{2-}]_{(s)} \qquad \text{Eq. (13)}$$

The best performance was achieved by applying a current density of 15.0 mA cm^{-2} (71.7%, final As^{3+} concentration of 70.6 ± 9.1 µg L^{-1}).

Conversely, a second EC system using iron electrodes achieved a complete elimination of arsenite, which was reached in less than 5 min of treatment at all applied current densities as shown in **Figure 18B**. The best performance for the abatement of As^{3+} in this EC system was at j = 6.0 mA cm^{-2} in 3 min of treatment. Then, EC tests at j= 5.0 and 4.0 mA cm^{-2} during 4 and 5 min, respectively, reached a complete abatement. Iron electrodes had better affinity to eliminate arsenic from wastewater compared with aluminum electrodes as it is reported by several studies (Nidheesh & Singh, 2017; Sandoval et al., 2021; Syam Babu & Nidheesh, 2021). This last is attributed to a direct and fast charge transfer oxidation from As^{3+} to As^{5+} (Sık et al., 2015; You & Han, 2016). The redox equations that represent the anodic process are the following:

At the anode, $Fe_{(s)} \rightarrow Fe_{(aq)}^{2+} + 2e^-$ Eq. (14)

The electrogeneration of Fe^{3+} is favored by reacting with oxygen species in solution (Eq. (15) and (16)) to produce FeOOH and $Fe(OH)_3$ (Eq. (17) and (18)) which are the preferred species to remove arsenic species (Sandoval et al., 2021; Syam Babu et al., 2021).

$4Fe^{2+}_{(aq)} + 4H^{+} + O_{2(g)} \rightarrow 4Fe^{3+}_{(aq)} + 2H_2O_{(l)}$, in acid media Eq. (15)

$4Fe^{2+}_{(aq)} + 2H_2O_{(l)} + O_{2(g)} \rightarrow 4Fe^{3+}_{(aq)} + 4OH^{-}$, in alkaline media Eq. (16)

$4Fe(OH)_{2(s)} + 2H_2O_{(l)} + O_{2(g)} \rightarrow 4Fe(OH)_{3(s)}$ Eq. (17)

$Fe(OH)_{3(s)} \rightarrow FeOOH_{(s)} + H_2O_{(l)}$ Eq. (18)

Moreover, although rare, further oxidation from Fe^{2+} to Fe^{4+} could influence the oxidation of inorganic As^{3+} and the generation of Fe^{3+} (Montefalcon et al., 2020).

The coagulating hydroxylated Fe^{3+} species with high charge density form insoluble flocs on which the adsorption of the As species occurs as can be seen in Eqs. (19-21). At the same time, at the cathode, the formation of

gaseous hydrogen promotes the floating of electrogenerated solids and also favors the mass transfer in the adsorption process of the inorganic As in the flocs.

$$Fe(OH)_{3(s)} + AsO_4^{3-}{}_{(aq)} \rightarrow Fe(OH)_3 * AsO_4^{3-}{}_{(s)} \quad \text{Eq. (19)}$$

$$2FeOOH_{(s)} + H_2AsO_4^-{}_{(aq)} \rightarrow (FeO)_2HAsO_{4(s)} + H_2O_{(l)} + OH^-{}_{(aq)}$$

Eq. (20)

$$3FeOOH_{(s)} + HAsO_4^{2-}{}_{(aq)} \rightarrow (FeO)_3AsO_{4(s)} + H_2O_{(l)} + 2OH^-{}_{(aq)}$$

Eq. (21)

Furthermore, arsenite concentration is lower than QL (42.89 µg L^{-1} As^{3+}) after 2 min of treatment. Therefore, the residual arsenite concentration could not be assessed because it was not statistically reliable if under that of QL. Arsenic concentration was measured by GFAAS, which found a post-treatment concentration of 64.91 µg L^{-1} (RSD 13.14%) when using Al electrodes with a *j* of 15.0 mA cm^{-2} for 60 min, and 1.44 µg L^{-1} (RSD 11.62%) when employing Fe electrodes and 6.0 mA cm^{-2}, for 3 min of treatment. Therefore, the concentrations measured with the electrochemical

methodology developed in this work were contrasted with the reference technique GFAAS.

Figure 19 (a) and (c) show SEM images obtained by aluminum electrodes (15.0 mA cm^{-2}, 60 min) and iron electrodes (6.0 mA cm^{-2}, 5 min), respectively. SEM images show flocs with an irregular morphology, with micrometric sizes between 50 and 10 µm for aluminum electrodes and sizes less of 20 µm for iron electrodes. These differences may be attributed to the electrolysis time. As commented previously, aluminum EC treatment required one hour before observing a decrease in arsenic concentration, while using iron as a working electrode, the EC process required only 5 minutes for the complete abatement. Then, longer electrocoagulation times promote larger flocs. **Figure 19** (b) and (d) display the FTIR spectra of aluminum and iron flocs after EC treatment, respectively. The FTIR analyses were performed in the 4000 – 450 cm^{-1} range to analyze the chemical bonds present in the obtained flocs. Both infrared spectrums show a wide band at 3260 – 3280, which corresponds to the O-H stretching vibrations (Sandoval et al., 2019). In the case of aluminum flocs, the peak located at 2981 cm^{-1} corresponds to Al-S-O bending, the 1120 cm^{-1} peak corresponds to Na-Al,

and Al-O may be represented at 1070 cm^{-1}. The arsenic bonds present in the flocs may be represented by the peaks observed at 948 cm^{-1}, which are O-As-O bonds; the As-OH is located at 631 cm^{-1} and the peak at 599 cm^{-1}, likely corresponding to the As-O bond (Purenović et al., 2011). In turn, the iron flocs analyzed by FTIR show a band at 595 cm^{-1} corresponding to $Fe^{2+}Fe^{3+}O_4$ interactions, and a Fe-O bond represented by 470 cm^{-1} band. The arsenic interactions in the flocs are represented by different peaks: As-O bond are showed in the band of 2854 cm^{-1}, at 890 cm^{-1} peak, representing the Na-As-O bond, As-OH peak are present at 620 cm^{-1} and finally, an iron-arsenic interaction appeared at the 872 cm^{-1} peak, which was attributed to Fe-O-As and As^{5+}-O interactions (Jia et al., 2007). Both FTIR spectra confirm the removal of arsenic from the fortified effluent by the adsorption process (Di Iorio et al., 2018) and the formation of complex metallic compounds (Nandiyanto et al., 2019). Other interactions with the metallic compounds with Na and S can be observed due to the effluent composition.

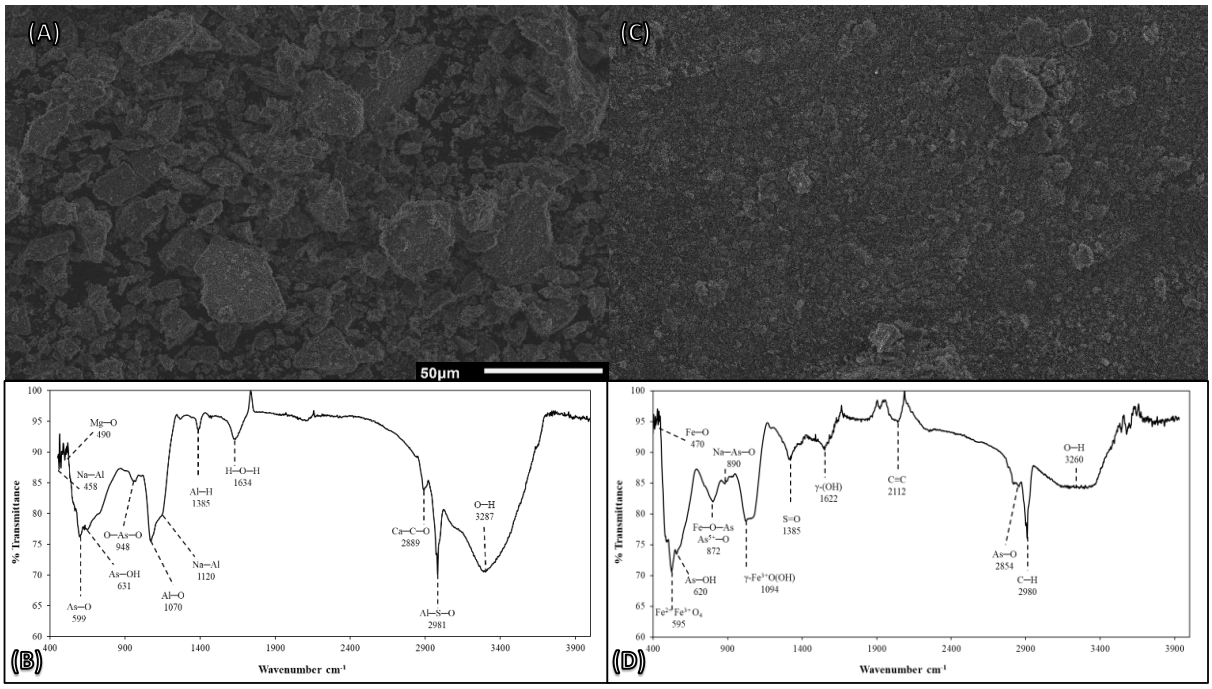

Figura 19: SEM micrographs (A) and FTIR spectra (B) of aluminum flocs obtained from the EC process at 15.0 mA cm^2 and 60 minutes of treatment; and SEM micrographs (C) and FTIR spectra (D) of iron flocs obtained from EC process at 6.0 mA cm^2 and 5 minutes of treatment.

XRF analyses were carried out to confirm the presence of arsenic in the flocs obtained through EC treatment, confirming the presence of the major compounds present in the flocs. In the case of aluminum flocs, aluminum (338000 ppm), sulfur (62600 ppm), chloride (40000 ppm), calcium (24400

ppm), copper (186 ppm), sodium (68000 ppm) and arsenic (29.3 ppm) were found in the samples. In turn, the principal compounds present in the iron flocs are sulfur (22100 ppm), chloride (70800 ppm), calcium (32600 ppm), iron (640000 ppm) and arsenic (13 ppm). Both analyses confirm the removal of arsenite from the treated effluent and the concentration of the pollutants on the flocs generated by EC treatment (Jia et al., 2007).

Finally, XRD analyzes were performed on the flocs obtained by the electrocoagulation process. **Figure 20A** shows the X ray diffraction pattern of the flocs obtained at *j* of 15.0 mA cm^{-2} for 60 min. using aluminum electrodes for EC. In this case, the diffractogram shows broad peaks due to the overlapping of peaks of other unidentified crystalline compounds formed during the treatment. Peaks corresponding to the following phases could be identified: Boehmite AlO(OH), Halite (NaCl), Anhydrite ($CaSO_4$), and Calcium Sulfate ($CaSiO_4$). On the other hand, **Figure 20B** shows the X ray diffraction pattern of the flocs obtained at *j* of 6.0 mA cm^{-2} for 5 min using steel electrodes for EC. Peaks corresponding to the following phases could be identified: Magnetite (Fe_3O_4), Halite (NaCl), Maghemite (Fe_3O_4), Anhydrite ($CaSO_4$), and Wallastonite ($CaSiO_3$). The XRD results presented

could indicate that the removal of arsenic is carried out by adsorption and trapping of the contaminant in amorphous structures, since no peaks are observed in the diffractogram that reveal the formation of crystalline arsenic compounds.

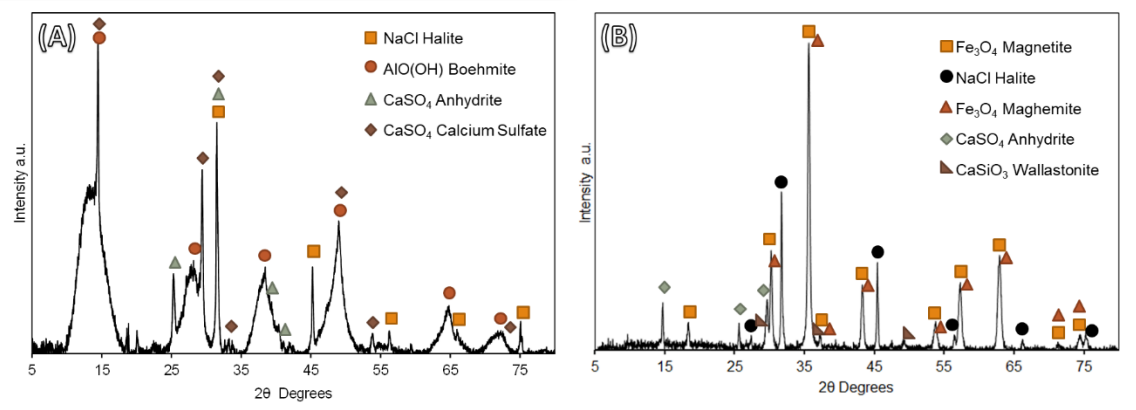

Figura 20: X ray diffraction pattern of the flocs obtained at *j* of 15.0 mA cm^{-2} for 60 min. using aluminum electrodes (A) and X ray diffraction pattern of the flocs obtained at *j* of 6.0 mA cm^{-2} for 5 min. using steel electrodes (B).

4.2.4. Conclusions

The new MWCNT-NH_2/AuNP sensor developed in this work showed an improvement in terms of signal-to-noise ratio, sensitivity, and selectivity compared with functionalized MWCNTs-modified GCE or a non-functionalized GCE. The application of an electrochemical methodology for arsenite quantification in a complex environmental matrix showed a high sensitivity (19.58 nA L μg^{-1}) and sufficient LD (0.39 $\mu g\ L^{-1}$) when using the MWCNT-NH_2/AuNP, confirming the possible use for monitoring/controlling arsenite concentration. Furthermore, the developed methodology was proved in monitoring the removal of arsenite in real WWTP effluent spiked with of 250 $\mu g\ L^{-1}$ As^{3+}.

This study act as a starting point to explore the use of nanostructured electrodes for direct and on-site analysis of polluted groundwater and surface water in rapid, sensitive, and easy setup procedure.

5. CONCLUSIONES

- El uso de heteroestructuras conformadas por nanotubos de carbono funcionalizados y AuNPs para la modificación de electrodos de carbono vitreo permite obtener electrodos modificados con mayor área electroactiva que la de un electrodo de carbono vitreo o de electrodos modificados solamente con nanotubos de carbono, lo que se evidencia en el aumento de la sensibilidad y la relación señal-ruido al utilizar métodos electroanalíticos para el análisis de matrices de interés medioambiental como aguas naturales, agua potable, efluentes y riles, de compuestos orgánicos electroactivos como dihidroxibencenos y metales pesados como el arsénico.

- Independiente de la naturaleza química de los compuestos estudiados, el potencial de pico obtenido se desplaza hacia potenciales menos anódicos, debido al efecto electrocatalítico ejercido por las AuNP utilizadas para la modificación de los electrodos. Este desplazamiento

de pico favorece la separación de las señales anódicas obtenidas por compuestos que pueden presentar un potencial de oxidación similar. En este caso, fue posible la determinación simultanea de los isómeros hidroquinona y catecol, logrando separar los picos de ambos isómeros (ΔE_{pa}= 100 mV), en riles, aguas naturales y aguas de consumo humano con alto efecto de matriz, pudiendo cuantificar ambos compuestos en un rango de trabajo entre 10.0 a 150.0 µM.

- El análisis de matrices ambientales reales fue posible mediante el uso de adición estándar en la mayoría de los casos, logrando minimizar el efecto de matriz en la determinación de los analitos estudiados. En el caso del análisis de dihidroxibencenos en riles vitivinícolas esta metodología de calibración presento bajos índices de recuperación (>52.3%), por lo que se aplicó un criterio de calibración multivariado basado en PLS, donde se construyó un modelo de calibración de manera prospectiva para evaluar la utilización de este tipos de herramientas quimiométricas para lograr la cuantificación de estos analitos a pesar del elevado efecto de matriz con errores de predicción menores al 10%, según los resultados obtenidos. En el futuro se

propone explorar la aplicación de este tipo de herramientas quimiométricas a datos electroquímicos obtenidos por técnicas cuantitativas, como DPV, donde se puede aumentar el numero de muestras de calibración para mejorar la robustez del modelo y disminuir los errores de predicción. También es posible la utilización de métodos de preprocesamiento de los voltamogramas, como filtros de suavizado de Savitzky-Golay y la derivación de los voltamogramas para superar los problemas de reproducibilidad que presentan este tipo de técnicas y que dificultan la aplicación de herramientas quimiométricas de calibración multivariada.

- La aplicación de una metodología electroquímica para la cuantificación de arsénico a niveles de µg L^{-1} fue exitosa, logrando una alta sensibilidad (19.58 nA L μg^{-1}) al utilizar MWCNT-NH_2/AuNP como superficie electródica, donde fue posible el análisis de arsénico en un rango de 42.89 – 170.00 µg L^{-1} en efluentes secundarios. También se realizó el seguimiento de un tratamiento de electrocoagulación, utilizado para la remoción de arsénico de aguas contaminadas, siendo esta aplicación el punto de partida para explorar

el uso de electrodos nanoestructurados para el análisis en terreno de aguas contaminadas con arsénico o para el seguimiento de tratamientos aplicados en plantas de tratamiento de aguas, donde este tipo de técnicas tienen el potencial de uso para realizar análisis de tipo "screening" y/o análisis cuantitativo, mediante técnicas electroquímicas que entregan respuestas rápidas, sensibles y con capacidad de portabilidad.

6. REFERENCIAS

Abid, R., Manzoor, M., De Oliveira, L. M., da Silva, E., Rathinasabapathi, B., Rensing, C., Mahmood, S., Liu, X., & Ma, L. Q. (2019). Interactive effects of As, Cd and Zn on their uptake and oxidative stress in As-hyperaccumulator Pteris vittata. *Environmental Pollution*, *248*, 756–762. https://doi.org/10.1016/j.envpol.2019.02.054

Afrooz, A. R. M. N., Das, D., Murphy, C. J., Vikesland, P., & Saleh, N. B. (2016). Co-transport of gold nanospheres with single-walled carbon nanotubes in saturated porous media. *Water Research*, *99*, 7–15. https://doi.org/10.1016/j.watres.2016.04.006

Ahammad, A. J. S., Akter, T., Al Mamun, A., Islam, T., Hasan, M., Mamun, M. A., Faraezi, S., Monira, F. Z., & Saha, J. K. (2018). Cost-effective electrochemical sensor based on carbon nanotube modified-pencil electrode for the simultaneous determination of hydroquinone and catechol. *Journal of the Electrochemical Society*, *165*(9), B390–B397. https://doi.org/10.1149/2.1341809jes

Alharbi, O. M. L., Basheer, A. A., Khattab, R. A., & Ali, I. (2018). Health and environmental effects of persistent organic pollutants. *Journal of Molecular Liquids*, *263*, 442–453. https://doi.org/10.1016/j.molliq.2018.05.029

Alim, S., Vejayan, J., Yusoff, M. M., & Kafi, A. K. M. (2018a). Recent uses of carbon nanotubes & gold nanoparticles in electrochemistry with application in biosensing: A review. *Biosensors and Bioelectronics*, *121*(July), 125–136. https://doi.org/10.1016/j.bios.2018.08.051

Alim, S., Vejayan, J., Yusoff, M. M., & Kafi, A. K. M. (2018b). Recent uses of carbon nanotubes

& gold nanoparticles in electrochemistry with application in biosensing: A review. *Biosensors and Bioelectronics*, *121*(August), 125–136. https://doi.org/10.1016/j.bios.2018.08.051

Alshahrani, L. A., Liu, L., Sathishkumar, P., Nan, J., & Gu, F. L. (2018). Copper oxide and carbon nano-fragments modified glassy carbon electrode as selective electrochemical sensor for simultaneous determination of catechol and hydroquinone in real-life water samples. *Journal of Electroanalytical Chemistry*, *815*, 68–75. https://doi.org/10.1016/j.jelechem.2018.03.004

Antonova, S., & Zakharova, E. (2016). Inorganic arsenic speciation by electroanalysis. From laboratory to field conditions: A mini-review. *Electrochemistry Communications*, *70*, 33–38. https://doi.org/10.1016/j.elecom.2016.06.011

Anuar, N. S., Basirun, W. J., Ladan, M., Shalauddin, M., & Mehmood, M. S. (2018). Fabrication of platinum nitrogen-doped graphene nanocomposite modified electrode for the electrochemical detection of acetaminophen. *Sensors and Actuators, B: Chemical*, *266*, 375–383. https://doi.org/10.1016/j.snb.2018.03.138

Aragó, M., Ariño, C., Dago, À., Díaz-Cruz, J. M., & Esteban, M. (2016). Simultaneous determination of hydroquinone, catechol and resorcinol by voltammetry using graphene screen-printed electrodes and partial least squares calibration. *Talanta*, *160*, 138–143. https://doi.org/10.1016/j.talanta.2016.07.007

Asere, T. G., Stevens, C. V., & Du Laing, G. (2019). Use of (modified) natural adsorbents for arsenic remediation: A review. *Science of the Total Environment*, *676*, 706–720. https://doi.org/10.1016/j.scitotenv.2019.04.237

Ávila, C., & García, J. (2015). Persistent Organic Pollutants (POPs): Analytical Techniques, Environmental Fate and Biological Effects. In *Comprehensive Analytical Chemistry* (Vol. 67). https://doi.org/10.1016/B978-0-444-63299-9.00006-5

Bansal, S., Priyanka, Bhandari, R., & Dharamvira, K. (2016). Study of gold nanostructures of various dimensions: Au NWs, Au nanosheets, Au nanocylinders. *Materials Today: Proceedings*, *3*(6), 2232–2240. https://doi.org/10.1016/j.matpr.2016.04.131

Beckers, F., & Rinklebe, J. (2017). Cycling of mercury in the environment: Sources, fate, and human health implications: A review. *Critical Reviews in Environmental Science and Technology*, *47*(9), 693–794. https://doi.org/10.1080/10643389.2017.1326277

Belghiti, D. K., Scorsone, E., & Bergonzo, P. (2016). Metal Nanoparticles/BDD Hybrid Electrodes for Analytical Detection of Pollutants in Water. *MRS Advances*, *1*(16), 1131–1136. https://doi.org/10.1557/adv.2016.171

Bounegru, A. V., & Apetrei, C. (2020). Voltammetric sensors based on nanomaterials for detection of caffeic acid in food supplements. *Chemosensors*, *8*(2). https://doi.org/10.3390/CHEMOSENSORS8020041

Buffa, A., & Mandler, D. (2019). Arsenic(III) detection in water by flow-through carbon nanotube membrane decorated by gold nanoparticles. *Electrochimica Acta*, *318*, 496–503. https://doi.org/10.1016/j.electacta.2019.06.114

Bullen, J. C., Torres-Huerta, A., Salaün, P., Watson, J. S., Majumdar, S., Vilar, R., & Weiss, D. J. (2020). Portable and rapid arsenic speciation in synthetic and natural waters by an As(V)-selective chemisorbent, validated against anodic stripping voltammetry. *Water Research*, *175*, 115650. https://doi.org/10.1016/j.watres.2020.115650

Calzadilla, W., Espinoza, L. C., Diaz-Cruz, M. S., Sunyer, A., Aranda, M., Peña-Farfal, C., & Salazar, R. (2021). Simultaneous degradation of 30 pharmaceuticals by anodic oxidation: Main intermediaries and by-products. *Chemosphere*, *269*(xxxx). https://doi.org/10.1016/j.chemosphere.2020.128753

Campbell, F. W., & Compton, R. G. (2010). The use of nanoparticles in electroanalysis: An updated review. *Analytical and Bioanalytical Chemistry*, *396*(1), 241–259. https://doi.org/10.1007/s00216-009-3063-7

Candia-Onfray, C., Thiam, A., Salazar, C., Martinez-Huitle, C. A., & Salazar, R. (2017). Enhanced Degradation of the Industrial Textile Dye Disperse Red BG by Electrochemical Process with Different Anodes. *Journal of The Electrochemical Society*, *164*(13), E440–E447. https://doi.org/10.1149/2.1101713jes

Cavanillas, S., Alberich, A., Serrano, N., Díaz-Cruz, J. M., Ariño, C., & Esteban, M. (2012). Application of different chemometric strategies to voltammetric and UV-vis spectroscopic data to obtain a complexation model: Study of the Cu(ii) binding with the phytohormone 6-benzylaminopurine. *Analyst*, *137*(22), 5420–5427. https://doi.org/10.1039/c2an35600g

Compton, Richard G. Batchelor-McAuley, C., & Dickinson, E. J. F. (2012). *Understanding Voltammetry : Problems and Solutions*. Imperial College Press. https://doi.org/https://doi.org/10.1142/p783

Cui, H., He, C. X., & Zhao, G. W. (1999). Determination of polyphenols by HPLC with inhibited chemiluminescence detection. *Journal of Chromatography A*, *855*(1), 171–179. file://reinette/bdd/BaseBiblio/Photocopies/9892.pdf

Currie, L. A. (1995). Nomenclature in evaluation of analytical methods including detection and quantification capabilities (IUPAC Recommendations 1995). *Pure and Applied Chemistry*, *67*(10), 1699–1723. https://doi.org/10.1351/pac199567101699

Di Iorio, E., Cho, H. G., Liu, Y., Cheng, Z., Angelico, R., & Colombo, C. (2018). Arsenate retention mechanisms on hematite with different morphologies evaluated using AFM, TEM measurements and vibrational spectroscopy. *Geochimica et Cosmochimica Acta*, *237*, 155–170. https://doi.org/10.1016/j.gca.2018.06.027

Diez, N. M., Cabanillas, A. G., Silva Rodríguez, A., & Goicoechea, H. C. (2015). Second-order advantage maintenance with voltammetric data modeling for quantitation of ethiofencarb in the presence of interferences. *Talanta*, *132*, 851–856. https://doi.org/10.1016/j.talanta.2014.10.006

Donini, C. A., da Silva, M. K. L., Simões, R. P., & Cesarino, I. (2018). Reduced graphene oxide modified with silver nanoparticles for the electrochemical detection of estriol. *Journal of Electroanalytical Chemistry*, *809*(August 2017), 67–73. https://doi.org/10.1016/j.jelechem.2017.12.054

EEA. (2013). DIRECTIVE OF THE EUROPEAN PARLIAMENT AND OF THE COUNCIL on the quality of water intended for human consumption. In *EUROPEAN COMMISSION* (Vol. 53, Issue 9). https://eur-lex.europa.eu/resource.html?uri=cellar:8c5065b2-074f-11e8-b8f5-01aa75ed71a1.0018.02/DOC_1&format=PDF

Electrochemical Strategies in Detection Science. (2015). https://doi.org/10.1039/9781782622529

Elghobashy, M. R., Bebawy, L. I., Shokry, R. F., & Abbas, S. S. (2016). Successive ratio subtraction coupled with constant multiplication spectrophotometric method for determination of hydroquinone in complex mixture with its degradation products, tretinoin and methyl paraben. *Spectrochimica Acta - Part A: Molecular and Biomolecular Spectroscopy*, *157*, 116–123. https://doi.org/10.1016/j.saa.2015.12.019

Escandar, G. M., Goicoechea, H. C., Muñoz de la Peña, A., & Olivieri, A. C. (2014). Second- and higher-order data generation and calibration: A tutorial. *Analytica Chimica Acta*, *806*, 8–26. https://doi.org/10.1016/j.aca.2013.11.009

Escandar, G. M., & Olivieri, A. C. (2017). A road map for multi-way calibration models. *Analyst*, *142*(16), 2862–2873. https://doi.org/10.1039/c7an00822h

Feldmann, J. (2002). *Volatilization of Metals from a Landfill Site Antimony , Bismuth , Mercury , Arsenic , and Tellurium on a*. 128–140.

Feldmann, Jrög, Salaün, P., & Lombi, E. (2009). Critical review perspective: Elemental speciation analysis methods in environmental chemistry-moving towards methodological integration. *Environmental Chemistry*, *6*(4), 275–289. https://doi.org/10.1071/EN09018

Feng, J. J., Chen, S. S., Chen, X. L., Zhang, X. F., & Wang, A. J. (2018). One-pot fabrication of reduced graphene oxide supported dendritic core-shell gold@gold-palladium nanoflowers for glycerol oxidation. *Journal of Colloid and Interface Science*, *509*, 73–81. https://doi.org/10.1016/j.jcis.2017.08.059

Ganesh, P. S., & Kumara Swamy, B. E. (2015). Simultaneous electroanalysis of hydroquinone and catechol at poly(brilliant blue) modified carbon paste electrode: A voltammetric study. *Journal of Electroanalytical Chemistry*, *756*, 193–200. https://doi.org/10.1016/j.jelechem.2015.08.027

Garcia-Costa, A. L., Sarabia, A., Zazo, J. A., & Casas, J. A. (2021). UV-assisted Catalytic Wet Peroxide Oxidation and adsorption as efficient process for arsenic removal in groundwater. *Catalysis Today*, *361*(May 2020), 176–182. https://doi.org/10.1016/j.cattod.2020.03.054

Gholivand, M. B., Jalalvand, A. R., Goicoechea, H. C., Gargallo, R., Skov, T., & Paimard, G. (2015). Combination of electrochemistry with chemometrics to introduce an efficient analytical method for simultaneous quantification of five opium alkaloids in complex matrices. *Talanta*, *131*, 26–37. https://doi.org/10.1016/j.talanta.2014.07.053

Gholivand, M. B., Jalalvand, A. R., Goicoechea, H. C., & Skov, T. (2014). Chemometrics-assisted simultaneous voltammetric determination of ascorbic acid, uric acid, dopamine and nitrite: Application of non-bilinear voltammetric data for exploiting first-order advantage. *Talanta*, *119*, 553–563. https://doi.org/10.1016/j.talanta.2013.11.028

Ghoreishi, S. M., Behpour, M., Hajisadeghian, E., & Golestaneh, M. (2012). Voltammetric determination of resorcinol on the surface of a glassy carbon electrode modified with multi-walled carbon nanotube. *Arabian Journal of Chemistry*. https://doi.org/10.1016/j.arabjc.2012.04.009

Gorchev, H. G., & Ozolins, G. (1984). WHO guidelines for drinking- water quality. *WHO Chronicle*, *38*(3), 104–108.

Goren, A. Y., & Kobya, M. (2021). Arsenic removal from groundwater using an aerated electrocoagulation reactor with 3D Al electrodes in the presence of anions. *Chemosphere*, *263*, 128253. https://doi.org/10.1016/j.chemosphere.2020.128253

Goren, A. Y., Kobya, M., & Oncel, M. S. (2020). Arsenite removal from groundwater by aerated electrocoagulation reactor with Al ball electrodes: Human health risk assessment. *Chemosphere*, *251*, 126363. https://doi.org/10.1016/j.chemosphere.2020.126363

Govindasamy, M., Manavalan, S., Chen, S.-M., Rajaji, U., Chen, T.-W., Al-Hemaid, F. M. A., Ali, M. A., & Elshikh, M. S. (2018). Determination of Neurotransmitter in Biological and Drug Samples Using Gold Nanorods Decorated f- MWCNTs Modified Electrode . *Journal of The Electrochemical Society*, *165*(9), B370–B377. https://doi.org/10.1149/2.1351809jes

Guo, H., Zhang, B., Wang, G., & Shen, Z. (2010). Geochemical controls on arsenic and rare earth elements approximately along a groundwater flow path in the shallow aquifer of the Hetao Basin, Inner Mongolia. *Chemical Geology*, *270*(1–4), 117–125. https://doi.org/10.1016/j.chemgeo.2009.11.010

Gupta, S., Murthy, C. N., & Prabha, C. R. (2018). Recent advances in carbon nanotube based electrochemical biosensors. *International Journal of Biological Macromolecules*, *108*, 687–703. https://doi.org/10.1016/j.ijbiomac.2017.12.038

Han, H. S., You, J. M., Seol, H., Jeong, H., & Jeon, S. (2014). Electrochemical sensor for hydroquinone and catechol based on electrochemically reduced GO-terthiophene-CNT. *Sensors and Actuators, B: Chemical*, *194*, 460–469. https://doi.org/10.1016/j.snb.2014.01.006

Hou, L., Jiang, L., Song, Y., Ding, Y., Zhang, J., Wu, X., & Tang, D. (2016). Amperometric aptasensor for saxitoxin using a gold electrode modified with carbon nanotubes on a self-assembled monolayer, and methylene blue as an electrochemical indicator probe. *Microchimica Acta*, *183*(6), 1971–1980. https://doi.org/10.1007/s00604-016-1836-1

Hu, Y., Li, D., Tang, P., Bin, Y., & Wang, H. (2019). Materials & Design Comparative study of structure , mechanical and electromagnetic interference shielding properties of carbon nanotube buckypapers prepared by different dispersion media. *Materials & Design*, *184*, 108175. https://doi.org/10.1016/j.matdes.2019.108175

Hung, D. Q., Nekrassova, O., & Compton, R. G. (2004). Analytical methods for inorganic arsenic in water: A review. *Talanta*, *64*(2), 269–277. https://doi.org/10.1016/j.talanta.2004.01.027

Hussain, C. M., & Kharisov, B. (2017). *Advanced Environmental Analysis* (Vol. 1, Issue December). https://doi.org/10.1039/9781782623625

Jain, C. K., & Ali, I. (2000). Arsenic: Occurrence, toxicity and speciation techniques. *Water Research*, *34*(17), 4304–4312. https://doi.org/10.1016/S0043-1354(00)00182-2

Jia, Y., Xu, L., Wang, X., & Demopoulos, G. P. (2007). Infrared spectroscopic and X-ray diffraction characterization of the nature of adsorbed arsenate on ferrihydrite. *Geochimica et Cosmochimica Acta*, *71*(7), 1643–1654. https://doi.org/10.1016/j.gca.2006.12.021

Jin, W., & Maduraiveeran, G. (2017). Electrochemical detection of chemical pollutants based on gold nanomaterials. *Trends in Environmental Analytical Chemistry*, *14*(April), 28–36.

https://doi.org/10.1016/j.teac.2017.05.001

Jin, Y., Wu, S., Zeng, Z., & Fu, Z. (2017). Effects of environmental pollutants on gut microbiota. *Environmental Pollution*, *222*, 1–9. https://doi.org/10.1016/j.envpol.2016.11.045

Jr, R. W. K., & Township, M. (2016). Arsenic : Properties and Determination. In *Encyclopedia of Food and Health* (1st ed., Issue 7440). Elsevier Ltd. https://doi.org/10.1016/B978-0-12-384947-2.00042-8

Kamyabi, M. A., & Aghaei, A. (2016). Electromembrane extraction coupled to square wave anodic stripping voltammetry for selective preconcentration and determination of trace levels of As(III) in water samples. *Electrochimica Acta*, *206*, 192–198. https://doi.org/10.1016/j.electacta.2016.04.127

Karim-Nezhad, G., Moghaddam, M. H., Khorablou, Z., & Dorraji, P. S. (2017). L-cysteine based polymer matrix decorated with au-nanoparticles: As a sensing platform for simultaneous determination of hydroquinone and catechol. *Journal of the Electrochemical Society*, *164*(6), B193–B199. https://doi.org/10.1149/2.0891706jes

Katz E, W. I., & Wang, J. (2004). Electroanalytical and bioelectroanalytical systems based on metal and semiconductor nanoparticles. *Electroanalysis*, *16*(1–2), 19–44. https://doi.org/10.1002/elan.200302930

Kooshki, H., Rashidiani, J., Kamali, M., Sedighian, H., Akbariqomi, M., & Mansouri, M. (2018). Ultrahigh sensitive enhanced-electrochemiluminescence detection of cancer biomarkers using silica NPs/graphene oxide: A comparative study. *Biosensors and Bioelectronics*, *102*, 226–233. https://doi.org/10.1016/j.bios.2017.11.011

Kooshki, M., Abdollahi, H., Bozorgzadeh, S., & Haghighi, B. (2011). Second-order data obtained from differential pulse voltammetry: Determination of tryptophan at a gold nanoparticles

decorated multiwalled carbon nanotube modified glassy carbon electrode. *Electrochimica Acta*, *56*(24), 8618–8624. https://doi.org/10.1016/j.electacta.2011.07.049

Kooshki, M., Díaz-Cruz, J. M., Abdollahi, H., Ariño, C., & Esteban, M. (2011). Asymmetric logistic peak as a suitable function for the resolution of highly asymmetric voltammograms in non-bilinear systems. *Analyst*, *136*(22), 4696–4703. https://doi.org/10.1039/c1an15396j

Kroukamp, E. M., Wondimu, T., & Forbes, P. B. C. (2016). Metal and metalloid speciation in plants: Overview, instrumentation, approaches and commonly assessed elements. *TrAC - Trends in Analytical Chemistry*, *77*, 87–99. https://doi.org/10.1016/j.trac.2015.10.007

Kumar, N., Bansal, A., Sarma, G. S., & Rawal, R. K. (2014). Chemometrics tools used in analytical chemistry: An overview. *Talanta*, *123*, 186–199. https://doi.org/10.1016/j.talanta.2014.02.003

Kumar, S., Bhanjana, G., Dilbaghi, N., Kumar, R., & Umar, A. (2016). Fabrication and characterization of highly sensitive and selective arsenic sensor based on ultra-thin graphene oxide nanosheets. *Sensors and Actuators, B: Chemical*, *227*, 29–34. https://doi.org/10.1016/j.snb.2015.11.101

Lalmalsawmi, J., Tiwari, D., & Kim, D. J. (2020). Role of nanocomposite materials in the development of electrochemical sensors for arsenic: Past, present and future. *Journal of Electroanalytical Chemistry*, *877*, 114630. https://doi.org/10.1016/j.jelechem.2020.114630

Lawal, A. T. (2018). Progress in utilisation of graphene for electrochemical biosensors. *Biosensors and Bioelectronics*, *106*(October 2017), 149–178. https://doi.org/10.1016/j.bios.2018.01.030

Lee, I., Jeong, G. H., An, S., Kim, S. W., & Yoon, S. (2018). Facile synthesis of 3D MnNi-layered double hydroxides (LDH)/graphene composites from directly graphites for pseudocapacitor

and their electrochemical analysis. *Applied Surface Science*, *429*, 196–202. https://doi.org/10.1016/j.apsusc.2017.06.259

Li, J., Xia, J., Zhang, F., Wang, Z., & Liu, Q. (2018). An electrochemical sensor based on copper-based metal-organic frameworks-graphene composites for determination of dihydroxybenzene isomers in water. *Talanta*, *181*(October 2017), 80–86. https://doi.org/10.1016/j.talanta.2018.01.002

Li, R., Liu, L., Zhu, H., & Li, Z. (2018). Synthesis of gold-palladium nanowaxberries/dodecylamine-functionalized graphene quantum dots-graphene micro-aerogel for voltammetric determination of peanut allergen Ara h 1. *Analytica Chimica Acta*, *1008*, 38–47. https://doi.org/10.1016/j.aca.2018.01.031

Li, Y., Li, Z., Liu, H., Chen, S., Guo, X., Lin, M., & Li, F. (2019). A Portable Electrochemical Platform Integrated with a 3D AuNPs/CNTs Sponge for Point-of-Care Testing of Neurotransmitters. *Journal of The Electrochemical Society*, *166*(6), B524–B531. https://doi.org/10.1149/2.1361906jes

Liu, K., Wang, X., Ntziachristos, V., Marsch, S., & Hunziker, P. (2017). Polymeric nanosystems for near-infrared multispectral photoacoustic imaging: Synthesis, characterization and in vivo evaluation. *European Polymer Journal*, *88*, 713–723. https://doi.org/10.1016/j.eurpolymj.2016.03.008

Liu, W., Tao, F., Zhang, W., Li, S., & Zheng, M. (2012). Contamination and emission factors of PCDD/Fs, unintentional PCBs, HxCBz, PeCBz and polychlorophenols in chloranil in China. *Chemosphere*, *86*(3), 248–251. https://doi.org/10.1016/j.chemosphere.2011.09.034

López-Lorente, Á. I. (2014). Gold Nanoparticles in Analytical Chemistry. In *Comprehensive Analytical Chemistry* (Vol. 66). https://doi.org/10.1016/B978-0-444-63285-2.00001-8

López, M. I., Callao, M. P., & Ruisánchez, I. (2015). A tutorial on the validation of qualitative methods: From the univariate to the multivariate approach. *Analytica Chimica Acta*, *891*, 62–72. https://doi.org/10.1016/j.aca.2015.06.032

Ma, J., Sengupta, M. K., Yuan, D., & Dasgupta, P. K. (2014). Speciation and detection of arsenic in aqueous samples: A review of recent progress in non-atomic spectrometric methods. *Analytica Chimica Acta*, *831*, 1–23. https://doi.org/10.1016/j.aca.2014.04.029

Masoum, S., Behpour, M., Azimi, F., & Motaghedifard, M. H. (2014). Potentiality of chemometric approaches for the determination of (+)-catechin in green tea leaves at the surface of multiwalled carbon nanotube paste electrode. *Sensors and Actuators, B: Chemical*, *193*, 582–591. https://doi.org/10.1016/j.snb.2013.12.022

Mendes, R. G., Wróbel, P. S., Bachmatiuk, A., Sun, J., Gemming, T., Liu, Z., & Rümmeli, M. H. (2018). Carbon nanostructures as a multi-functional platform for sensing applications. *Chemosensors*, *6*(4). https://doi.org/10.3390/chemosensors6040060

Mestrot, A., Planer-Friedrich, B., & Feldmann, J. (2013). Biovolatilisation: a poorly studied pathway of the arsenic biogeochemical cycle. *Environmental Science: Processes & Impacts*, *15*(9), 1639. https://doi.org/10.1039/c3em00105a

Mohammadi, G., Rashidi, K., Mahmoudi, M., Goicoechea, H. C., & Jalalvand, A. R. (2018). Exploiting second-order advantage from mathematically modeled voltammetric data for simultaneous determination of multiple antiparkinson agents in the presence of uncalibrated interference. *Journal of the Taiwan Institute of Chemical Engineers*, *88*, 49–61. https://doi.org/10.1016/j.jtice.2018.04.007

Moldoveanu, S. C., & Kiser, M. (2007). Gas chromatography/mass spectrometry versus liquid chromatography/fluorescence detection in the analysis of phenols in mainstream cigarette smoke. *Journal of Chromatography A*, *1141*(1), 90–97.

https://doi.org/10.1016/j.chroma.2006.11.100

Montefalcon, M. F. V., Chiong, M. R., Resurreccion, A. C., Garcia-Segura, S., & Ocon, J. D. (2020). Arsenic removal by advanced electrocoagulation processes: The role of oxidants generated and kinetic modeling. *Catalysts*, *10*(8), 1–16. https://doi.org/10.3390/catal10080928

Nandiyanto, A. B. D., Oktiani, R., & Ragadhita, R. (2019). How to read and interpret ftir spectroscope of organic material. *Indonesian Journal of Science and Technology*, *4*(1), 97–118. https://doi.org/10.17509/ijost.v4i1.15806

Naqvi, S. T. R., Rasheed, T., Hussain, D., Najam ul Haq, M., Majeed, S., shafi, S., Ahmed, N., & Nawaz, R. (2020). Modification strategies for improving the solubility/dispersion of carbon nanotubes. *Journal of Molecular Liquids*, *297*, 1–12. https://doi.org/10.1016/j.molliq.2019.111919

Ni, Y., & Kokot, S. (2008). Does chemometrics enhance the performance of electroanalysis? *Analytica Chimica Acta*, *626*(2), 130–146. https://doi.org/10.1016/j.aca.2008.08.009

Nidheesh, P. V., & Singh, T. S. A. (2017). Arsenic removal by electrocoagulation process: Recent trends and removal mechanism. *Chemosphere*, *181*, 418–432. https://doi.org/10.1016/j.chemosphere.2017.04.082

Nigović, B., Jurić, S., & Mornar, A. (2018). Electrochemical determination of nepafenac topically applied nonsteroidal anti-inflammatory drug using graphene nanoplatelets-carbon nanofibers modified glassy carbon electrode. *Journal of Electroanalytical Chemistry*, *817*(March), 30–35. https://doi.org/10.1016/j.jelechem.2018.03.068

Nugent, J. M., Santhanam, K. S. V., Rubio, A., & Ajayan, P. M. (2001). Fast Electron Transfer Kinetics on Multiwalled Carbon Nanotube Microbundle Electrodes. *Nano Letters*, *1*(2), 87–

91. https://doi.org/10.1021/nl005521z

Núñez, C., Arancibia, V., & Triviño, J. J. (2018). A new strategy for the modification of a carbon paste electrode with carrageenan hydrogel for a sensitive and selective determination of arsenic in natural waters. *Talanta*, *187*, 259–264. https://doi.org/10.1016/j.talanta.2018.05.028

Odom, T. W., Huang, J. L., Kim, P., & Lieber, C. M. (1998). Atomic structure and electronic properties of single-walled carbon nanotubes. *Nature*, *391*(January), 62–64. https://doi.org/10.1038/34139

Olivieri, A. C. (2015). Practical guidelines for reporting results in single- and multi-component analytical calibration: A tutorial. *Analytica Chimica Acta*, *868*, 10–22. https://doi.org/10.1016/j.aca.2015.01.017

Omar, T. F. T., Ahmad, A., Aris, A. Z., & Yusoff, F. M. (2016). Endocrine disrupting compounds (EDCs) in environmental matrices: Review of analytical strategies for pharmaceuticals, estrogenic hormones, and alkylphenol compounds. *TrAC - Trends in Analytical Chemistry*, *85*, 241–259. https://doi.org/10.1016/j.trac.2016.08.004

Otto, M. (2017). *Chemometrics: Statics and Computer Application in Analytical Chemistry* (Third Edit). Wiley.

Patel, D. C., Patel, N. R., Sherikar, O. D., & Mehta, P. J. (2014). Development and validation of RP-HPLC, HPTLC and UV-visible spectrophotometric methods for simultaneous estimation of alprazolam and propranolol hydrochloride in their combined dosage form. *Journal of Analytical Chemistry*, *69*(7), 674–680. https://doi.org/10.1134/S1061934814070119

Patil, S. K., Patil, S. A., Vadiyar, M. M., Awale, D. V., Sartape, A. S., Walekar, L. S., Kolekar, G. B., Ghorpade, U. V., Kim, J. H., & Kolekar, S. S. (2017). Tailor-made dicationic ionic liquid

as a fluorescent sensor for detection of hydroquinone and catechol. *Journal of Molecular Liquids*, *244*, 39–45. https://doi.org/10.1016/j.molliq.2017.08.119

Peng, C., Li, Z., Zhang, X., Zhou, S., Zhang, W., Liu, X., & Zhao, P. (2018). Simultaneous Determination of Hydroquinone, Catechol and Resorcinol with High Selectivity Based on Hollow Nitrogen-Doped Mesoporous Carbon Spheres Decorated Graphene. *Journal of The Electrochemical Society*, *165*(5), B212–B219. https://doi.org/10.1149/2.0801805jes

Peng, L. M., Zhang, Z., & Wang, S. (2014). Carbon nanotube electronics: Recent advances. *Materials Today*, *17*(9), 433–442. https://doi.org/10.1016/j.mattod.2014.07.008

Pereira, F. J., Vázquez, M. D., Debán, L., & Aller, A. J. (2016a). Inorganic arsenic speciation by differential pulse anodic stripping voltammetry using thoria nanoparticles-carbon paste electrodes. *Talanta*, *152*, 211–218. https://doi.org/10.1016/j.talanta.2016.02.011

Pereira, F. J., Vázquez, M. D., Debán, L., & Aller, A. J. (2016b). Inorganic arsenic speciation by differential pulse anodic stripping voltammetry using thoria nanoparticles-carbon paste electrodes. *Talanta*, *152*, 211–218. https://doi.org/10.1016/j.talanta.2016.02.011

Petursdottir, A. H., Sloth, J. J., & Feldmann, J. (2015). Introduction of regulations for arsenic in feed and food with emphasis on inorganic arsenic, and implications for analytical chemistry. *Analytical and Bioanalytical Chemistry*, *407*(28), 8385–8396. https://doi.org/10.1007/s00216-015-9019-1

Pomerantsev, A. L., & Rodionova, O. Y. (2010). Chemometric view on "comprehensive chemometrics." *Chemometrics and Intelligent Laboratory Systems*, *103*(1), 19–24. https://doi.org/10.1016/j.chemolab.2010.05.001

Pravdová, V., Pravda, M., & Guilbault, G. G. (2002). Role of Chemometrics for Electrochemical Sensors. *Analytical Letters*, *35*(15), 2389–2419. https://doi.org/10.1081/AL-120016533

Promchan, J., Günther, D., Siripinyanond, A., & Shiowatana, J. (2016). Elemental imaging and classifying rice grains by using laser ablation inductively coupled plasma mass spectrometry and linear discriminant analysis. *Journal of Cereal Science*, *71*, 198–203. https://doi.org/10.1016/j.jcs.2016.08.017

Pu, S. Y., Zinchenko, A., Qin, L. L., Ye, C. W., Xu, M., & Murata, S. (2014). Photochemical metallization to fabricate DNA-templated gold nanorings. *Materials Letters*, *130*, 168–171. https://doi.org/10.1016/j.matlet.2014.05.066

Punetha, V. D., Rana, S., Yoo, H. J., Chaurasia, A., McLeskey, J. T., Ramasamy, M. S., Sahoo, N. G., & Cho, J. W. (2017). Functionalization of carbon nanomaterials for advanced polymer nanocomposites: A comparison study between CNT and graphene. *Progress in Polymer Science*, *67*, 1–47. https://doi.org/10.1016/j.progpolymsci.2016.12.010

Punrat, E., Chuanuwatanakul, S., Kaneta, T., Motomizu, S., & Chailapakul, O. (2013). Method development for the determination of arsenic by sequential injection/anodic stripping voltammetry using long-lasting gold-modified screen-printed carbon electrode. *Talanta*, *116*, 1018–1025. https://doi.org/10.1016/j.talanta.2013.08.030

Purenović, J., Mitić, V. V., Paunović, V., & Purenović, M. (2011). Microstructure characterization of porous microalloyed aluminium-silicate ceramics. *Journal of Mining and Metallurgy, Section B: Metallurgy*, *47*(2), 157–169. https://doi.org/10.2298/JMMB110331011P

Qin, L., Zeng, G., Lai, C., Huang, D., Xu, P., Zhang, C., Cheng, M., Liu, X., Liu, S., Li, B., & Yi, H. (2018). "Gold rush" in modern science: Fabrication strategies and typical advanced applications of gold nanoparticles in sensing. *Coordination Chemistry Reviews*, *359*, 1–31. https://doi.org/10.1016/j.ccr.2018.01.006

Raab, A., Stiboller, M., Gajdosechova, Z., Nelson, J., & Feldmann, J. (2016). Element content and daily intake from dietary supplements (nutraceuticals) based on algae, garlic, yeast fish and

krill oils—Should consumers be worried? *Journal of Food Composition and Analysis*, *53*, 49–60. https://doi.org/10.1016/j.jfca.2016.09.008

Rao, H., Zhao, X., Liu, X., Zhong, J., Zhang, Z., Zou, P., Jiang, Y., Wang, X., & Wang, Y. (2018). A novel molecularly imprinted electrochemical sensor based on graphene quantum dots coated on hollow nickel nanospheres with high sensitivity and selectivity for the rapid determination of bisphenol S. *Biosensors and Bioelectronics*, *100*, 341–347. https://doi.org/10.1016/j.bios.2017.09.016

Rodrígúez-Lado, L., Sun, G., Berg, M., Zhang, Q., Xue, H., Zheng, Q., & Johnson, C. A. (2013). Groundwater arsenic contamination throughout China. *Science*, *341*(6148), 866–868. https://doi.org/10.1126/science.1237484

RSC Publishing. (2013). *Nanoscience* (Vol. 1). https://doi.org/10.1039/9781849734844

Salunke, R. S., Nakate, Y. T., Umar, A., Nakate, U. T., Ahmad, R., & Shirale, D. J. (2021). Anodic stripping voltammetry analysis of gold nanoparticles functionalized one-dimensional single polypyrrole nanowire for arsenic sensing. *Surfaces and Interfaces*, *23*(October 2020), 100895. https://doi.org/10.1016/j.surfin.2020.100895

Sandoval, M. A., Fuentes, R., Nava, J. L., Coreño, O., Li, Y., & Hernández, J. H. (2019). Simultaneous removal of fluoride and arsenic from groundwater by electrocoagulation using a filter-press flow reactor with a three-cell stack. *Separation and Purification Technology*, *208*, 208–216. https://doi.org/10.1016/j.seppur.2018.02.018

Sandoval, M. A., Fuentes, R., Thiam, A., & Salazar, R. (2021). Arsenic and fluoride removal by electrocoagulation process: A general review. *Science of the Total Environment*, *753*, 142108. https://doi.org/10.1016/j.scitotenv.2020.142108

Sebarchievici, I., Taranu, B. O., Birdeanu, M., Rus, S. F., & Fagadar-Cosma, E. (2016).

Electrocatalytic behaviour and application of manganese porphyrin/gold nanoparticle-surface modified glassy carbon electrodes. *Applied Surface Science*, *390*, 131–140. https://doi.org/10.1016/j.apsusc.2016.07.158

Sedghi, R., & Pezeshkian, Z. (2015). Fabrication of non-enzymatic glucose sensor based on nanocomposite of MWCNTs-COOH-Poly(2-aminothiophenol)-Au NPs. *Sensors and Actuators B: Chemical*, *219*, 119–124. https://doi.org/10.1016/j.snb.2015.04.097

Sık, E., Kobya, M., Demirbas, E., Oncel, M. S., & Goren, A. Y. (2015). Removal of As(V) from groundwater by a new electrocoagulation reactor using Fe ball anodes: optimization of operating parameters. *Desalination and Water Treatment*, *56*(5), 1177–1190. https://doi.org/10.1080/19443994.2014.951691

Skaldina, O., Peräniemi, S., & Sorvari, J. (2018). Ants and their nests as indicators for industrial heavy metal contamination. *Environmental Pollution*, *240*, 574–581. https://doi.org/10.1016/j.envpol.2018.04.134

Sullivan, C., Lu, D., Senecal, A., & Kurup, P. (2021). Voltammetric Detection of Arsenic (III) using Gold Nanoparticles Modified Carbon Screen Printed Electrodes: Application for Facile and Rapid Analysis in Commercial Apple Juice. *Food Chemistry*, *Iii*, 129327. https://doi.org/10.1016/j.foodchem.2021.129327

Suvarapu, L. N., & Baek, S.-O. (2016). Current Research on the Speciation and Determination of Mercury in Different Environmental Matrices Using Various Analytical Instruments. *Doi.Org*, *2017*. https://doi.org/10.20944/preprints201609.0015.v1

Syam Babu, D., & Nidheesh, P. V. (2021). A review on electrochemical treatment of arsenic from aqueous medium. *Chemical Engineering Communications*, *208*(3), 389–410. https://doi.org/10.1080/00986445.2020.1715956

Syam Babu, D., Vijay, K., Nidheesh, P. V., & Suresh Kumar, M. (2021). Performance of continuous aerated iron electrocoagulation process for arsenite removal from simulated groundwater and management of arsenic-iron sludge. *Sustainable Energy Technologies and Assessments*, *47*(September 2020), 101476. https://doi.org/10.1016/j.seta.2021.101476

Taheran, M., Naghdi, M., Brar, S. K., Verma, M., & Surampalli, R. Y. (2018). Emerging contaminants: Here today, there tomorrow! *Environmental Nanotechnology, Monitoring and Management*, *10*(May), 122–126. https://doi.org/10.1016/j.enmm.2018.05.010

Tashkhourian, J., Daneshi, M., Nami-Ana, F., Behbahani, M., & Bagheri, A. (2016a). Simultaneous determination of hydroquinone and catechol at gold nanoparticles mesoporous silica modified carbon paste electrode. *Journal of Hazardous Materials*, *318*, 117–124. https://doi.org/10.1016/j.jhazmat.2016.06.049

Tashkhourian, J., Daneshi, M., Nami-Ana, F., Behbahani, M., & Bagheri, A. (2016b). Simultaneous determination of hydroquinone and catechol at gold nanoparticles mesoporous silica modified carbon paste electrode. *Journal of Hazardous Materials*, *318*, 117–124. https://doi.org/10.1016/j.jhazmat.2016.06.049

Thirumalraj, B., Kubendhiran, S., Chen, S.-M., & Lin, K.-Y. (2017). Highly sensitive electrochemical detection of palmatine using a biocompatible multiwalled carbon nanotube/poly- l -lysine composite. *Journal of Colloid and Interface Science*, *498*, 144–152. https://doi.org/10.1016/j.jcis.2017.03.045

Toothaker, R. D., Wright, D. S., & Pachla, L. A. (1987). *MINIREVIEW Recent Analytical Methods for Cephalosporins in Biological Fluids*. *31*(8), 1157–1163.

Trachioti, M. G., Karantzalis, A. E., Hrbac, J., & Prodromidis, M. I. (2019). Low-cost screen-printed sensors on-demand: Instantly prepared sparked gold nanoparticles from eutectic Au/Si alloy for the determination of arsenic at the sub-ppb level. *Sensors and Actuators, B:*

Chemical, *281*, 273–280. https://doi.org/10.1016/j.snb.2018.10.112

Tserpes, K., & Silvestre, N. (2014). Modeling of Carbon Nanotubes , Graphene and their Composites. In *Springer Series in Materials Science*. Springer International Publishing.

Turkevich, John; Cooper, P. H. J. (1951). A study of the nucleation and growth process in the synthesis of colloidal gold. *Discussions of the Faraday Society*, *55*(c), 55–75. https://doi.org/10.1039/df9511100055

Turkevich, J., Stevenson, P. C., & Hillier, J. (1951). A study of the nucleation and growth processes in the synthesis of colloidal gold. *Discussions of the Faraday Society*, *11*(c), 55–75. https://doi.org/10.1039/DF9511100055

Urgast, D. S., Beattie, J. H., & Feldmann, J. (2014). Imaging of trace elements in tissues: With a focus on laser ablation inductively coupled plasma mass spectrometry. *Current Opinion in Clinical Nutrition and Metabolic Care*, *17*(5), 431–439. https://doi.org/10.1097/MCO.0000000000000087

US-EPA. (2001). *Arsenic Rule Technical Fact Sheet* (pp. 1–6). https://www.epa.gov/dwreginfo/chemical-contaminant-rules

Vilela, C. L. S., Bassin, J. P., & Peixoto, R. S. (2018). Water contamination by endocrine disruptors: Impacts, microbiological aspects and trends for environmental protection. *Environmental Pollution*, *235*, 546–559. https://doi.org/10.1016/j.envpol.2017.12.098

Vytřas, K., Ashrafi, A. M., Švancara, I., Dalmacija, B., Rončević, S., Beljin, J., Kónya, Z., Guzsvány, V., Petrović, S., & Ranković, N. (2018). Trace level voltammetric determination of Zn(II) in selected nutrition related samples by bismuth-oxychloride-multiwalled carbon nanotube composite based electrode. *Microchemical Journal*, *146*(November 2018), 178–186. https://doi.org/10.1016/j.microc.2018.12.053

Wang, Jinshou, Yang, J., Xu, P., Liu, H., Zhang, L., Zhang, S., & Tian, L. (2020). Gold nanoparticles decorated biochar modified electrode for the high-performance simultaneous determination of hydroquinone and catechol. *Sensors and Actuators, B: Chemical*, *306*(April 2019), 127590. https://doi.org/10.1016/j.snb.2019.127590

Wang, Joseph. (2005). Carbon-nanotube Based Electrochemical Biosensors: A Review. *Electroanalysis*, *17*(1), 7–14. https://doi.org/10.1002/elan.200403113

Wang, M., Cui, M., Zhao, M., & Cao, H. (2018). Sensitive determination of Amaranth in foods using graphene nanomeshes. *Journal of Electroanalytical Chemistry*, *809*(August 2017), 117–124. https://doi.org/10.1016/j.jelechem.2017.12.059

Wildgoose, G. G., Banks, C. E., & Compton, R. G. (2006). Metal Nanoparticles and Related Materials Supported on Carbon Nanotubes: Methods and Applications. *Small*, *2*(2), 182–193. https://doi.org/10.1002/smll.200500324

Wong, A., Foguel, M. V., Khan, S., Oliveira, F. M. De, Tarley, C. R. T., & Sotomayor, M. D. P. T. (2015). Development of an Electrochemical Sensor Modified With MWCNT-COOH and MIP for Detection of Diuron. *Electrochimica Acta*, *182*, 122–130. https://doi.org/10.1016/j.electacta.2015.09.054

Wong, A., Santos, A. M., Silva, T. A., & Fatibello-Filho, O. (2018). Simultaneous determination of isoproterenol, acetaminophen, folic acid, propranolol and caffeine using a sensor platform based on carbon black, graphene oxide, copper nanoparticles and PEDOT:PSS. *Talanta*, *183*(February), 329–338. https://doi.org/10.1016/j.talanta.2018.02.066

Wu, Y. H., Imae, T., & Ujihara, M. (2017). Surface enhanced plasmon effects by gold nanospheres and nanorods in Langmuir-Blodgett films. *Colloids and Surfaces A: Physicochemical and Engineering Aspects*, *532*(February), 213–221. https://doi.org/10.1016/j.colsurfa.2017.05.015

Xia, H., Bai, S., Hartmann, J., & Wang, D. (2010). Synthesis of monodisperse quasi-spherical gold nanoparticles in water via silver(I)-assisted citrate reduction. *Langmuir*, *26*(5), 3585–3589. https://doi.org/10.1021/la902987w

Xiao, L., Wildgoose, G. G., & Compton, R. G. (2008). Sensitive electrochemical detection of arsenic (III) using gold nanoparticle modified carbon nanotubes via anodic stripping voltammetry. *Analytica Chimica Acta*, *620*(1–2), 44–49. https://doi.org/10.1016/j.aca.2008.05.015

Xiao, Y., Xu, L., Li, P., Tang, X. C., & Qi, L. W. (2017). A simple microdroplet chip consisting of silica nanochannel-assisted electrode and paper cover for highly sensitive electrochemiluminescent detection of drugs in human serum. *Analytica Chimica Acta*, 1–7. https://doi.org/10.1016/j.aca.2017.06.014

Xie, X., Johnson, T. M., Wang, Y., Lundstrom, C. C., Ellis, A., Wang, X., & Duan, M. (2013). Mobilization of arsenic in aquifers from the Datong Basin, China: Evidence from geochemical and iron isotopic data. *Chemosphere*, *90*(6), 1878–1884. https://doi.org/10.1016/j.chemosphere.2012.10.012

Yang, C., Denno, M. E., Pyakurel, P., & Venton, B. J. (2015). Recent trends in carbon nanomaterial-based electrochemical sensors for biomolecules: A review. *Analytica Chimica Acta*, *887*, 17–37. https://doi.org/10.1016/j.aca.2015.05.049

Yang, H., Wu, S., Duan, Y., Fu, X., & Wu, J. (2012). Surface modification of CNTs and enhanced photocatalytic activity of TiO2coated on hydrophilically modified CNTs. *Applied Surface Science*, *258*(7), 3012–3018. https://doi.org/10.1016/j.apsusc.2011.11.029

Yang, M., Guo, Z., Li, L., Huang, Y., Liu, J., & Zhou, Q. (2016). *Sensors and Actuators B : Chemical Electrochemical determination of arsenic (III) with ultra-high anti-interference performance using Au – Cu bimetallic nanoparticles*. *231*, 70–78.

https://doi.org/10.1016/j.snb.2016.03.009

You, H. J., & Han, I. S. (2016). Effects of dissolved ions and natural organic matter on electrocoagulation of As(III) in groundwater. *Journal of Environmental Chemical Engineering*, *4*(1), 1008–1016. https://doi.org/10.1016/j.jece.2015.12.034

Zakaria, A. B. M., & Leszczynska, D. (2019). Electrochemically prepared unzipped single walled carbon nanotubes-MnO2 nanostructure composites for hydrogen peroxide and glucose sensing. *Chemosensors*, *7*(1). https://doi.org/10.3390/CHEMOSENSORS7010001

Żelechowska, K., Trawiński, B., Dramińska, S., Majdecka, D., Bilewicz, R., & Kusz, B. (2017). Oxygen biosensor based on carbon nanotubes directly grown on graphitic substrate. *Sensors and Actuators B: Chemical*, *240*, 1308–1313. https://doi.org/10.1016/j.snb.2016.09.081

Zhai, C., Sun, X., Zhao, W., Gong, Z., & Wang, X. (2013). Acetylcholinesterase biosensor based on chitosan/prussian blue/multiwall carbon nanotubes/hollow gold nanospheres nanocomposite film by one-step electrodeposition. *Biosensors and Bioelectronics*, *42*(1), 124–130. https://doi.org/10.1016/j.bios.2012.10.058

Zhang, Ya, & Zheng, J. Bin. (2007). Comparative investigation on electrochemical behavior of hydroquinone at carbon ionic liquid electrode, ionic liquid modified carbon paste electrode and carbon paste electrode. *Electrochimica Acta*, *52*(25), 7210–7216. https://doi.org/10.1016/j.electacta.2007.05.039

Zhang, Yang, & Kang, Z. (2018). Highly conductive and anticorrosion Ag/CNTs/NDs hybrid films on molecular-grafted PET substrate for flexible electrodes. *Applied Surface Science*, *427*, 282–292. https://doi.org/10.1016/j.apsusc.2017.07.270

Zhao, L., Yu, J., Yue, S., Zhang, L., Wang, Z., Guo, P., & Liu, Q. (2018). Nickel oxide/carbon nanotube nanocomposites prepared by atomic layer deposition for electrochemical sensing

of hydroquinone and catechol. *Journal of Electroanalytical Chemistry*, *808*(September 2017), 245–251. https://doi.org/10.1016/j.jelechem.2017.12.019

Zheng, X., Fan, R., Hu, Y., Zhong, H., Yang, X., Lv, R., Yang, X., & Huang, B. (2020). Selective and simultaneous determination of hydroquinone and catechol by using a nitrogen-doped bagasse activated carbon modified electrode. *Materials Chemistry and Physics*, *242*(September 2019), 122525. https://doi.org/10.1016/j.matchemphys.2019.122525

Zhou, Q., Wang, W., Xiao, J., Wang, J., Liu, G., Shi, Q., & Guo, G. (2006). *Original Paper Comparison of the Enrichment Efficiency of Multiwalled Carbon Nanotubes , C18 Silica , and Activated Carbon as the Adsorbents for the Solid Phase Extraction of Atrazine and Simazine in Water Samples*. *224*, 215–224. https://doi.org/10.1007/s00604-005-0448-y

Zhou, X., He, Z., Lian, Q., Li, Z., Jiang, H., & Lu, X. (2014). Simultaneous determination of dihydroxybenzene isomers based on graphene-graphene oxide nanocomposite modified glassy carbon electrode. *Sensors and Actuators, B: Chemical*, *193*, 198–204. https://doi.org/10.1016/j.snb.2013.11.085

Zhou, Y., Huang, X., Zhang, W., Ji, Y., Chen, R., & Xiong, Y. (2018). Multi-branched gold nanoflower-embedded iron porphyrin for colorimetric immunosensor. *Biosensors and Bioelectronics*, *102*(November 2017), 9–16. https://doi.org/10.1016/j.bios.2017.10.046